

## AD-A263 706



ion is estimated to average 1 hour per response, including the time for reviewing instructions, searching existing data sources, gathering and reviewing the collection of information. Send comments regarding this burden estimate or any other aspect of this reporting burden, to Washington Headquarters Services, Directorate for Information Operations and Reports, 1215 Jefferson Avenue, S.W., Washington, D.C. 20540, and to the Office of Management and Budget, Paperwork Reduction Project (0704-0188), Washington, DC 20503.

2. REPORT DATE Feb 93	3. REPORT TYPE AND DATES COVERED Final 1 Jul 89-31 Dec 92
--------------------------	--

4. TITLE AND SUBTITLE  A Field Investigation of Water and Salt Movement in Permafrost and the Active Layer	5. FUNDING NUMBERS  DAAL03-89-K-0106
6. AUTHOR(S)  T.E. Osterkamp	8. PERFORMING ORGANIZATION REPORT NUMBER
7. PERFORMING ORGANIZATION NAME(S) AND ADDRESS(ES)  University of Alaska Fairbanks, Alaska 99775-0800	
9. SPONSORING/MONITORING AGENCY NAME(S) AND ADDRESS(ES)  U. S. Army Research Office P. O. Box 12211 Research Triangle Park, NC 27709-2211	10. SPONSORING/MONITORING AGENCY REPORT NUMBER  ARO 26281.5-GS

DTIC  
ELECTE  
MAY 06 1993  
S E D

11. SUPPLEMENTARY NOTES  The view, opinions and/or findings contained in this report are those of the author(s) and should not be construed as an official Department of the Army position, policy, or decision, unless so designated by other documentation.	
12a. DISTRIBUTION / AVAILABILITY STATEMENT  Approved for public release; distribution unlimited.	12b. DISTRIBUTION CODE

13. ABSTRACT (Maximum 200 words)  Evidence from subsea permafrost, permafrost in coastal regions of the Arctic and Antarctic, and in the cold and sometimes arid regions of China, the Soviet Union, Antarctica, and North America, indicates that saline permafrost is very widespread - perhaps more common than non-saline permafrost! This salty permafrost is found near the surface at depths of geotechnical interest, within, and under continuous and discontinuous permafrost. These salts can produce significant changes in permafrost properties and processes and it is possible for these salts to become mobile under potential energy gradients. It is concluded that saline permafrost will become increasingly important in the rational assessment of scientific, engineering, environmental, and agricultural problems of the future.	
--	--

93 5 05 03 4

93-09741



4620

14. SUBJECT TERMS  Permafrost, Subsea Permafrost, Saline Permafrost, Non-saline Permafrost			16. PRICE CODE
17. SECURITY CLASSIFICATION OF REPORT  UNCLASSIFIED	18. SECURITY CLASSIFICATION OF THIS PAGE  UNCLASSIFIED	19. SECURITY CLASSIFICATION OF ABSTRACT  UNCLASSIFIED	20. LIMITATION OF ABSTRACT  UL

FINAL REPORT

**A Field Investigation of Water and Salt Movement in  
Permafrost and the Active Layer**

by  
T.E. Osterkamp

February, 1993

Geophysical Institute  
University of Alaska  
Fairbanks, AK 99775-0800

Accession For	
NTIS CRA&I	<input checked="" type="checkbox"/>
DTIC TAB	<input type="checkbox"/>
Unannounced	<input type="checkbox"/>
Justification .....	
By .....	
Distribution /	
Availability Codes	
Dist	Avail and/or Special
A-1	

DTIC QUALITY INSPECTED 8

to

Army Research Office

for

ARO Proposal No. 26281-GS, Grant No. DAAL 03-89-K-0106

## SCIENTIFIC PERSONNEL SUPPORTED BY THE PROJECT

T.E. Osterkamp  
F.J. Wuttig  
T. Matava  
T. Zhang  
T. Fei  
R.E. Gilfilian

## DEGREES AWARDED

T. Matava, Ph.D. awarded, May, 1991. Thesis: Solute redistribution during freezing of sands saturated with saline solution.

T. Fei, M.S. awarded, May, 1992. Thesis: A theoretical study of the effects of sea level and climatic change on permafrost temperatures and gas hydrates.

T. Zhang, Ph.D. expected summer of 1993. Thesis: Changing climate and permafrost temperatures in Alaska.

## PUBLICATIONS AND PAPER PRESENTATIONS:

1. Osterkamp, T.E., Occurrence and potential importance of saline permafrost in Alaska, Paper presented to the Workshop on Saline Permafrost, Winnipeg, Manitoba, Oct. 26, 1989.
2. Osterkamp, T.E., Salt redistribution in freezing soils, Invited lecture, U.S. Army CRREL, Hanover, N.H., Oct. 31, 1989.
3. Zhang, T., T.E. Osterkamp, and J.P. Gosink, A model for the thermal regime of permafrost within the depth of annual temperature variations, Proc. of the Third Int. Symp. on Cold Regions Heat Transfer, Univ. of Alaska Fairbanks, Fairbanks, AK, June 1991.
4. Osterkamp, T.E., and T. Fei, Potential occurrence of permafrost and gas hydrates in the continental shelf near Lonely, Alaska, Accepted for publication in, Proc. of the Sixth Int. Conf. on Permafrost, Beijing, China, July, 1993.

5. Osterkamp, T.E., and T. Fei, Modeling the response of permafrost and gas hydrates to changes in sea level and climate, Proc. AAAS 43rd Arctic Sci. Conf., Valdez, AK, p. 36, Geophys. Inst., Univ. of Alaska, Fairbanks, AK, Sept. 1992.
6. Zhang, T., and T.E. Osterkamp, Modeling the response of permafrost to surface temperature changes in the Alaska Arctic, Proc. AAAS 43rd Arctic Sci. Conf., Valdez, AK, p.46, Geophys. Inst., Univ. of Alaska, Fairbanks, AK, Sept. 1992.
7. Zhang, T., and T.E. Osterkamp, Considerations in determining thermal diffusivity from temperature time series using numerical methods, paper submitted to Journal of Geophysical Research, November, 1992.
8. Wuttig, F.J., and T.E. Osterkamp, Water content and salt concentration profiles in warm permafrost, in preparation.
9. Osterkamp, T.E., and T. Fei, Effects of sea level and climatic change on permafrost in Alaska's continental shelves, in preparation.
10. Matava, T., T.E. Osterkamp, and J.R. Gosink, An experimental investigation of solute transport in saturated coarse-grained sands during freezing, in preparation.
11. A theoretical paper on salt redistribution in freezing soils is in preparation by Dr. T. Matava.

## OCCURRENCE AND POTENTIAL IMPORTANCE OF SALINE PERMAFROST IN ALASKA

T. E. Osterkamp  
Geophysical Institute  
University of Alaska  
Fairbanks, Alaska

### Introduction

Saline permafrost is defined to be permafrost with part or all of its water content unfrozen because of the salinity of the pore water. However, all soil pore water contains ions thus making all permafrost saline. Consequently, there is a need for a working definition of saline permafrost for geotechnical purposes. In this paper, permafrost with a pore water salinity greater than 1 ppt (part per thousand) or an electrical conductivity greater than,  $170 \text{ mS m}^{-1}$  will be considered saline.

This paper addresses the occurrence of saline permafrost, primarily in Alaska, its role in a few scientific and engineering problems, and suggests that saline permafrost may be much more common and more important than previously thought.

### Subsea Permafrost

Subsea permafrost is the most obvious and perhaps most extensive formation of saline permafrost. It has been found in the submerged continental shelves of the Arctic and Antarctic land masses where pore water salinities of shelf sediments may exceed that of the overlying seawater, especially in shallow water. These increased salinities are a result of the infiltration of salt derived from (rejected by) growing sea ice (Osterkamp et al., 1989). The study of subsea permafrost dynamics (i.e., its response to repetitive periods of submergence and emergence) is a scientific problem in its own right. Development of offshore petroleum reserves will require an increased knowledge of the geotechnical properties of subsea permafrost and of heat and matter flow processes in it.

### Coastal Regions

Saline permafrost might be expected in coastal areas as a result of airborne salts, seawater flooding, and variations in ground surface and sea levels over geologic time. Such occurrences have been found at Nome, Kotzebue, Barrow, Prudhoe Bay and at other sites along Alaska's extensive coast. Extremely high pore water salinities have been found at the surface, within, and under both continuous

and discontinuous permafrost in coastal areas (Osterkamp and Payne, 1981). Salinities exceeding 20 ppt have been found within 20 m of the surface (Figure 1). For comparison, annual sea ice typically has salinities of 5 to 10 ppt which gives some idea of the potential effects on the geotechnical and physical properties of the permafrost.

### Interior Regions

Observations of saline permafrost in the Alaska Interior have been accumulating. Holes drilled at Fairbanks, Eagle, Glennallen, and other sites along the pipeline corridor have found that the electrical conductivity of the pore water in the permafrost typically ranges from 100 to 300 mS m<sup>-1</sup>. Some sites have been found with values in the 500 to 1000 mS m<sup>-1</sup> range (Figure 2). At Happy Valley in the foothills north of the Brooks Range, saline permafrost (conductivity  $2.2 \times 10^3$  mS m<sup>-1</sup>) was found under an  $\approx$  12m thick layer of massive ice. There have also been reports of saline permafrost in the cold, arid regions of China, Soviet Union, and Antarctica. The papers presented at this workshop show that it is relatively common in Canada.

### Potential Importance

Why be concerned about the effects of salty pore water in permafrost? Salts modify the chemical potential of the pore water in the permafrost. As a result, there are changes in the phase equilibria conditions, especially freezing point, water film characteristics, and volume of unfrozen pore water at sub-zero temperatures. The salts may also modify the soil and ice structure; that of both pore ice and ice lenses. Salts can also be expected to be mobile, moving or concentrating under the influence of moisture, chemical, temperature, and hydraulic gradients. While the details of these effects are poorly known, it is known that saline pore water in permafrost causes marked changes in its physical and mechanical properties and in heat and matter flow processes especially during freezing or thawing.

Considering the widespread occurrence of saline permafrost, we can expect to encounter a growing number of scientific, engineering, environmental, and agricultural problems that require an understanding of saline permafrost for their rational assessment and evaluation.

### Summary

Evidence from subsea permafrost, permafrost in coastal regions of the Arctic and Antarctic, and in the cold and sometimes arid regions of China, the Soviet Union,

Antarctica, and North America, indicates that saline permafrost is very widespread - perhaps more common than non-saline permafrost! This salty permafrost is found near the surface at depths of geotechnical interest, within, and under continuous and discontinuous permafrost. We know that these salts can produce significant changes in permafrost properties and processes and that it is possible for these salts to become mobile under potential energy gradients. It is concluded that saline permafrost will become increasingly important in the rational assessment of scientific, engineering, environmental, and agricultural problems of the future.

#### References

- Osterkamp, T. E., G. C. Baker, W. D. Harrison, and T. Matava, Characteristics of the active layer and ice-bonded permafrost table of subsea permafrost, J. Geophysical Res., In press, Nov., 1989.
- Osterkamp, T. E., and M. W. Payne, Estimates of permafrost thickness from well logs in northern Alaska, Cold Reg. Sci. Tech., 5, 13-27, 1981.

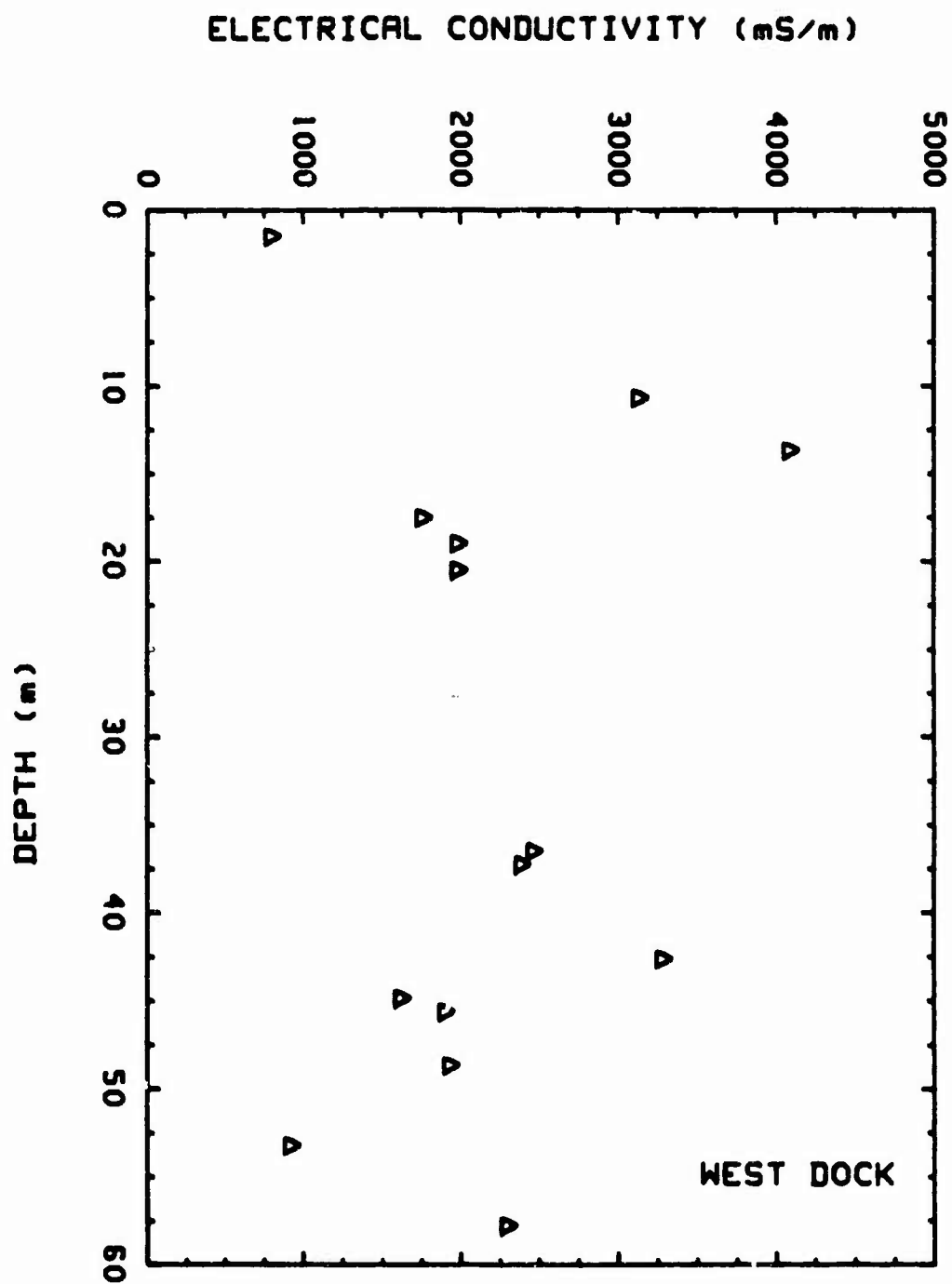


Figure 1. Electrical conductivity profile for pore water in permafrost near the West Dock, Prudhoe Bay, Alaska.

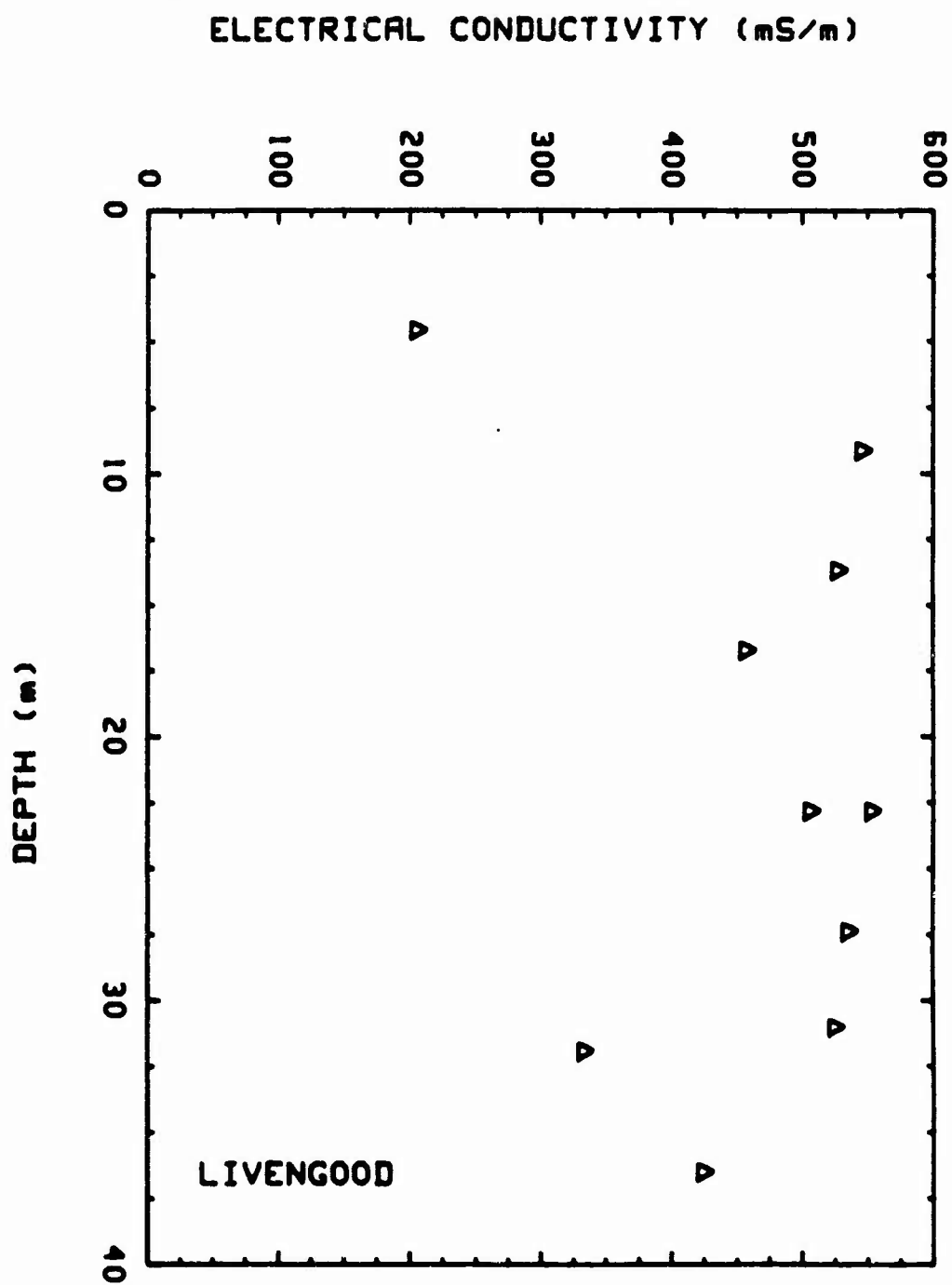


Figure 2. Electrical conductivity profile for pore water in permafrost near Livengood, Alaska.

U.S. Army Research Office and the Cold Regions Research and Engineering Laboratory  
72 Lyme Road, Hanover, New Hampshire 03755-1290

#

## SALT REDISTRIBUTION IN FREEZING SOILS

by

DR. TOM OSTERKAMP  
University of Alaska-Fairbanks  
Geophysical Research Institute

Date: Tuesday, 31 October 1989

Time: 10:30 a.m.

Location: Auditorium  
USA CRREL  
72 Lyme Road  
Hanover, New Hampshire

# **A Model for the Thermal Regime of Permafrost Within the Depth of Annual Temperature Variations**

T. Zhang, T. E. Osterkamp, and J. P. Gosink

Geophysical Institute  
University of Alaska Fairbanks  
Fairbanks, Alaska

## **ABSTRACT**

Temperature changes in permafrost within the depth of annual temperature variations are often modeled as a pure heat conduction problem in a homogeneous semi-infinite region with an equilibrium initial condition and a harmonic function of time representing seasonal changes in subsurface temperature. Continuous temperature measurements at the permafrost table show that the temperature there can be better approximated by a step or truncated cosine function. Analytical solutions of this heat conduction problem have been obtained for both step and truncated cosine boundary conditions. A temperature oscillation in the form of a step or truncated cosine function at the permafrost table gradually becomes sinusoidal with depth.

## **INTRODUCTION**

The thermal regime of permafrost within the depth of annual temperature variations is of importance for engineering design in cold regions. Soil temperatures are often modeled as a heat conduction problem in a semi-infinite region with a periodic surface temperature due to the periodic heating (both daily and annually). Temperature variations at the ground surface are usually approximated as a sinusoidal function of time and homogeneous soil materials are assumed (Carslaw and Jaeger, 1959; Lunardini, 1981)<sup>[1,2]</sup>. The solutions are applied to investigate daily and annual soil temperature variations (Oke, 1987)<sup>[3]</sup>, and permafrost problems in cold regions (Lunardini, 1981)<sup>[2]</sup>. However, for a wet active layer, the thermal history at the permafrost table cannot be exactly described by a sinusoidal boundary condition since the temperature there is constrained at or near 0°C for most of the thaw period (Lachenbruch et al., 1962; Zhang, 1989)<sup>[4, 5]</sup>.

Temperatures in permafrost are directly related to the temperature variations at the permafrost table and this supports the choice of the permafrost table as the upper boundary to investigate the thermal regime of permafrost. Measurements show that the temperature variations at the permafrost table can be approximated by a step or truncated cosine function (Lachenbruch et al., 1962; Zhang, 1989)<sup>[4,5]</sup>. This paper summarizes analytical solutions to the one-dimensional heat conduction equation in permafrost when the temperature variations at the permafrost table are represented by a step or a truncated cosine function.

## MATHEMATICAL MODELS

A step function,  $\varphi_1(t)$ , representation of the temperature at the permafrost table is, for the  $l$ 'th cycle,

$$\varphi_1(t) = \begin{cases} 0 & lP < t < lP + P_1 \\ T_o & lP + P_1 < t < lP + P_2 \\ 0 & lP + P_2 < t < (l+1)P \end{cases} \quad (1)$$

where  $t$  is the time in days,  $P$  is the period (one year), and  $P_1$  and  $P_2$  are the turn points in the step function. Equation (1) can be expanded in a Fourier's series

$$\varphi_1(t) = \frac{T_o(P_2 - P_1)}{P} + \sum_{n=1}^{\infty} A_n \cos\left(\frac{n\omega}{2}(2t - P_2 - P_1)\right) \quad (2)$$

where  $\omega = 2\pi/P$  and

$$A_n = \frac{2T_o}{n\pi} \sin\left(\frac{n\omega}{2}(P_2 - P_1)\right) \quad (3)$$

The first term on the right hand side of (2) is the mean annual temperature at the permafrost table,  $\bar{T}$ . Then, the mathematical model can be written in the form

$$\frac{\partial T}{\partial t} = D \frac{\partial^2 T}{\partial x^2} \quad (4)$$

$$T(x, 0) = \bar{T} + G_o x \quad (5)$$

$$T(0, t) = \bar{T} + \sum_{n=1}^{\infty} A_n \cos\left(\frac{n\omega}{2}(2t - P_2 - P_1)\right) \quad (6)$$

$$\lim_{x \rightarrow \infty} \frac{\partial T}{\partial x} = G_0 \quad (7)$$

where  $D$  is the thermal diffusivity in units of  $m^2 yr^{-1}$ ,  $x$  is the depth in  $m$  and  $G_0$  is the geothermal gradient in  $^{\circ}C m^{-1}$

The solution for (4) to (7) can be written in the form

$$T(x, t) = \bar{T} + G_0 x + \sum_{n=1}^{\infty} A_n e^{-xK} \cos\left(\frac{n\omega}{2}(2t - P_2 - P_1) - xK\right) - \frac{2}{\sqrt{\pi}} \int_0^{\frac{x}{2\sqrt{Dk}}} \sum_{n=1}^{\infty} A_n \cos\left(\frac{n\omega}{2}\left(2t - \frac{x^2}{4D\mu^2} - P_2 - P_1\right)\right) e^{-\mu^2} d\mu \quad (8)$$

where  $K = \sqrt{n\omega/2D}$ . The last term on the right hand side of (8) is the transient disturbance caused by starting the oscillations of surface temperature at time  $t = 0$ ; it dies away as  $t$  increases, leaving the third term which is the long term solution.

A truncated cosine function,  $\varphi_2(t)$ , can also be used to represent temperature variations at the permafrost table. For the  $l$ 'th cycle,

$$\varphi_2(t) = \begin{cases} 0 & lP < t < lP + P_1' \\ A_0 \cos(\omega t) + T_m & lP + P_1' < t < lP + P_2' \\ 0 & lP + P_2' < t < (l+1)P \end{cases} \quad (9)$$

where  $A_0$  is the amplitude of the cosine function in units of  $^{\circ}C$ ,  $T_m$  is the mean value of the cosine function during the entire period of  $P$  and is not in general equal to  $\bar{T}$ . Expanding (9) in a Fourier's series

$$\varphi_2(t) = \frac{a_0}{2} + \sum_{n=1}^{\infty} A_n' \cos(\omega n t - \varepsilon_n) \quad (10)$$

where  $A_n' = \sqrt{a_n^2 + b_n^2}$ ,  $\varepsilon_n = \tan^{-1}(b_n/a_n)$  and the  $a_n$  and  $b_n$  are the Fourier coefficients for the truncated cosine function.

The first term on the right hand side of (10) is  $\bar{T}$ . Then,

$$T(x,0) = \bar{T} + G_0 x \quad (11)$$

and

$$T(0,t) = \bar{T} + \sum_{n=1}^{\infty} A_n' \cos(\omega n t - \epsilon_n) \quad (12)$$

The steady-periodic solution for (4), (11) and (12) can be written in the form

$$T(x,t) = \bar{T} + G_0 x + \sum_{n=1}^{\infty} A_n' e^{-xK} \cos(\omega n t - \epsilon_n). \quad (13)$$

## RESULTS AND DISCUSSION

The first term on the right hand side of (8) and (13) is  $\bar{T}$ . The second term is the initial temperature variation with depth. The third term is the temperature oscillation around the mean temperature as a function of depth and time. Figure 1 shows the results calculated by (8) and (13), respectively for late June. The two solutions agree at depth (greater than 10 m or so) but generally disagree near the permafrost surface. A truncated cosine function is a better fit to measured temperatures (Zhang, 1989)<sup>[5]</sup> so that it is preferred over a step function although a step function is simpler to use. It is also preferred over a full cosine function which introduces too much warmth during the summer thaw period.

Figures 2 and 3 show the calculated annual oscillation of temperature at various depths as a result of the step and truncated cosine boundary conditions, respectively. The step and truncated cosine curves in Figures 2 and 3 are the boundary conditions with  $n = 200$  and the rest of the curves are the temperature oscillation with time at depths from 2 to 10 m with an increment of 2 m for  $n = 100$ . The "wiggles" in the step curve near  $P_1$  and  $P_2$  in Figure 2 or  $P_1'$  and  $P_2'$  in Figure 3 are caused by taking a finite number of terms in the series in (6) and (12).

The amplitude of the temperature oscillation at the permafrost table in (8) is

$$A_s = \sum_{n=1}^{\infty} \frac{2T_s}{n\pi} \sin\left(\frac{n\omega}{2}(P_2 - P_1)\right) \quad (14)$$

and in (12) it is

$$A_s = \sum_{n=1}^{\infty} A_n' \quad (15)$$

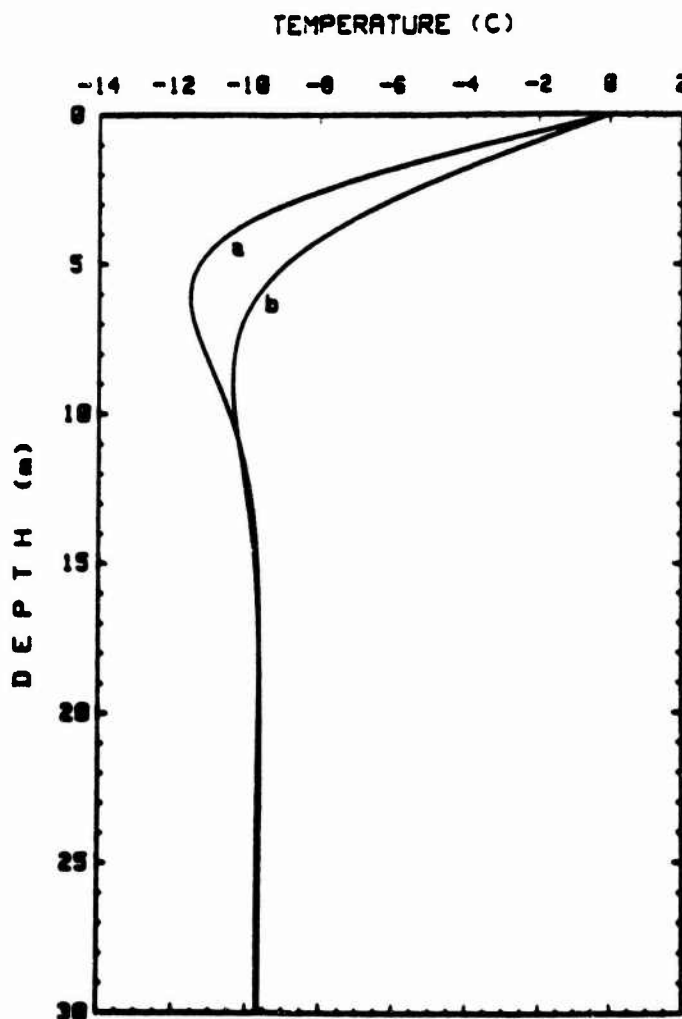


Figure 1: Temperature variation of permafrost with depth for late June calculated for solutions with a step (a) and truncated cosine (b) boundary conditions with  $P_1=70$  days,  $P_2=195$  days,  $P_1'=46$  days,  $P_2'=319$  days, and  $D=42.0 \text{ m}^2\text{yr}^{-1}$  starting from September 12.

and these amplitudes decrease with depth according to  $\sum_{n=1}^{\infty} e^{-\sqrt{n\omega/2D}}$ . Since  $D$  and  $\omega$  are assumed constant, when  $n$  increases, the wave number  $K$  increases and wave length  $\lambda=2\pi/K$  decreases until the higher harmonics die out for  $n$  sufficiently large. The higher harmonics in (8) and (13) disappear rapidly moving downwards into

the permafrost and the step and truncated cosine functions soon become sinusoidal. Figures 2 and 3 show that the amplitude of the temperature oscillation decreases with depth and that the shape of the curves approach a sinusoidal function at depth. Comparing Figure 2 with Figure 3, the higher harmonics in (13) disappear much faster than those in (8).

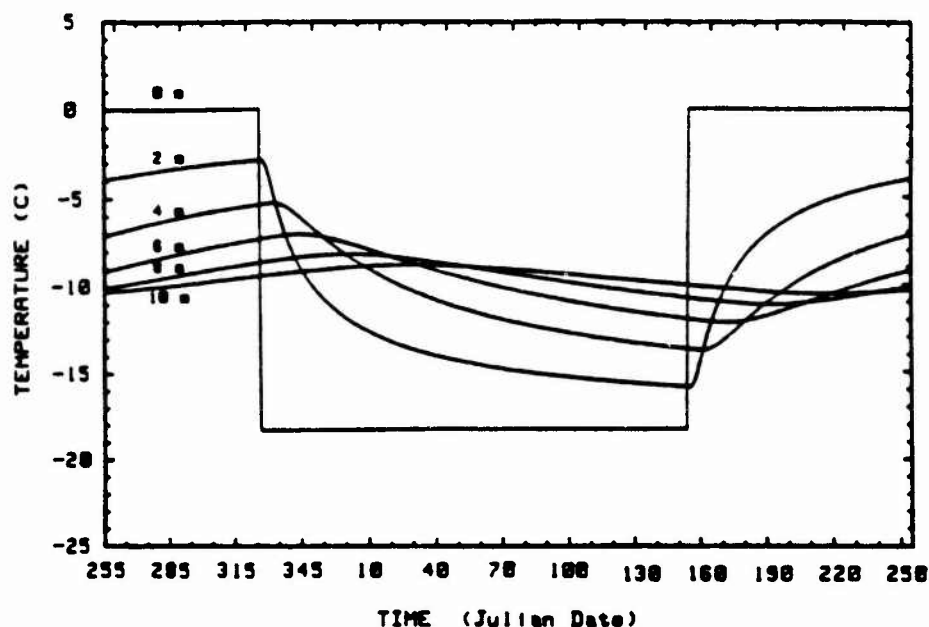


Figure 2: Annual oscillation of temperature at 2, 4, 6, 8, and 10 m caused by a step boundary condition at the permafrost table ( $x=0$ ).

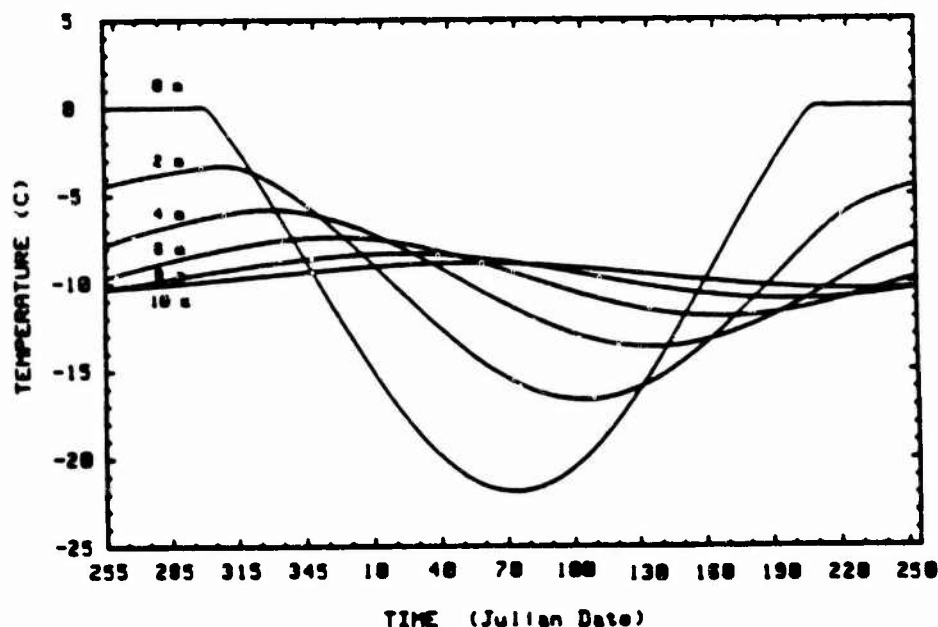


Figure 3: Annual oscillation of temperature at 2, 4, 6, 8, and 10 m by a truncated cosine boundary condition at the permafrost table ( $x=0$ ).

## CONCLUSIONS

The thermal regime of permafrost within the depth of the annual temperature variations is often analyzed as a pure heat conduction problem in a homogeneous semi-infinite region with the boundary condition a sine or cosine function of time at the ground surface to represent the change of seasons. However, for a wet active layer, the thermal regime of permafrost cannot be exactly described by a sinusoidal boundary condition at the ground surface due to phase change in the active layer over permafrost. The choice of the permafrost table as the upper boundary for investigating the thermal regime of permafrost overcomes this problem. Temperature measurements at the permafrost table show that the temperature variations there are not a sinusoidal function of time since the temperature is constrained at or near 0°C for part of the year. The measured data show that the temperature variation at the permafrost table can be better approximated as a step or a truncated cosine function. Analytical solutions to the heat conduction problem were obtained by expanding the assumed permafrost surface temperature variation in a Fourier series. The truncated cosine function at the surface is more realistic than the step function. When  $n$ , the number of terms, is large, the higher harmonics in the solutions are less important and disappear rapidly with depth in the permafrost. Both the step and truncated cosine function at the permafrost surface approach a sinusoidal function with depth.

## ACKNOWLEDGEMENTS

This research was sponsored by the Earth Sciences Section, Division of Polar Programs, National Science Foundation under grants DPP 86-19382 and DPP 87-21966 and by the U.S. Army Research Office, Contract DAAL03-89-K-0106.

## REFERENCES

1. Carslaw, H. S. and J. C. Jaeger, Conduction of heat in solids, second edition, 510 pp. Oxford at the Clarendon Press, 1959.
2. Lunardini, V. J., Heat Transfer in cold climates, 731 pp. Van Nostrand Reinhold Company, New York, 1981.
3. Oke, T. R., Boundary layer climates, second edition, 435 pp. Methuen, New York, 1987.
4. Lachenbruch, A. H., M. C. Brewer, G. W. Greene, and B. V. Marshall, Temperatures in permafrost, in Temperature-Its measurement and control, Vol. 3., part 1, p. 791-803, Reinhold Pub. Corp. New York, NY, 1962.
5. Zhang, T., Thermal regime of permafrost within the depth of annual temperature variation at Prudhoe Bay, Alaska, M. S. Thesis, University of Alaska, Fairbanks, Alaska, 1989.

= 4

POTENTIAL OCCURRENCE OF PERMAFROST AND GAS HYDRATES  
IN THE CONTINENTAL SHELF NEAR LONELY, ALASKA

T.E. Osterkamp and T. Fei

Geophysical Institute  
University of Alaska Fairbanks  
Fairbanks, Alaska 99775-0800

A two-dimensional finite element model was used to investigate the thermal response of subsea permafrost and gas hydrates to changes in sea level and climate over a 121 Kyr time period along a line offshore from Lonely, Alaska. For subsea permafrost containing brines, the spatial distribution of the ice-bearing permafrost (IBP) is predicted to be wedge shaped and to extend only 19 km offshore. There is significant lateral heat flow throughout the IBP section offshore and the depth to the IBP table increases almost linearly with distance offshore. For subsea permafrost with constant thermal parameters, IBP is predicted to extend 52 km offshore (water depth ~ 50 m) and is nearly isothermal beyond 4 km offshore. Depth to the IBP table increases almost linearly with distance offshore and then becomes relatively shallow and nearly constant in depth. Seabed temperatures and the assumed sea level history curve are especially important in determining the current distribution of subsea permafrost. The full thickness of IBP onshore can be modeled better using constant thermal parameters. Depth to the IBP table offshore may be modeled better when it is assumed that the permafrost contains brines. The predicted depth zone for stability of methane gas hydrates is between 220 m and 650 m near shore. For subsea permafrost containing brines, this zone extends 32 km offshore compared to 54 km (to the 55 m water depth) for constant thermal parameters. The time scale for producing methane gas from destabilized gas hydrates in the continental shelf near Lonely is on the order of  $10^4$  years, much longer than previously predicted.

## INTRODUCTION

During the past million years, there is evidence for repeated glaciations about every 10<sup>5</sup> years (Shackleton and Opdyke, 1977). The continental shelves of the Arctic Ocean were emergent during these glaciations, up to current water depths of 120 m (Bard et al., 1990). Cold climates during periods of emergence favored the formation of permafrost and the stabilization of gas hydrates in the shelves. Rising sea levels during interglacial periods replaced the cold air temperatures on the shelves by much warmer sea water temperatures. As a result, the permafrost and thawed sediments would have warmed at all depths, and permafrost would have started to thaw from both the top and the bottom. Eventually, gas hydrates would have been destabilized, providing a potential source of methane gas to the atmosphere.

Since permafrost thaws very slowly in response to the new surface boundary conditions after submergence, considerable time (on the order of tens of millennia) may be required to completely thaw the permafrost. Consequently, ice-bearing permafrost (IBP) and gas hydrates may still exist in parts of the continental shelves of the Arctic Ocean. The existence of subsea permafrost and the presence of ice in these continental shelves has been confirmed by drilling in shallow water (usually a few tens of meters or less in depth) off the coasts of the USSR (Molochushkin, 1978), Alaska (Lewellen, 1973), and Canada (Mackay, 1972). Subsea permafrost is also indicated in the interpretations of offshore seismic data (Hunter et al., 1976) and of geophysical logs in offshore petroleum exploration wells (Osterkamp et al., 1985). Destabilization of gas hydrates (by warming the sediments in the continental shelves) during periods of high sea level may be a periodic source of atmospheric methane over geological time (Clarke et al., 1986; MacDonald, 1990). Warming of the permafrost and sediments and permafrost

thawing eventually causes gas hydrates to become unstable resulting in the liberation of large volumes of gas. However, the permafrost may act as a seal (because of ice in the pores) preventing the gases from escaping until sufficient ice has been thawed to generate escape routes for the gas. MacDonald (1990) has investigated the time scales for the response of the permafrost to submergence using a one-dimensional analytical model. Since the model did not include latent heat effects, the predicted time scales are expected to be much too short. This means that his predictions regarding the time scales for production of atmospheric methane gas by destabilization of gas hydrates in continental shelves affected by permafrost are not correct.

Calculations using one-dimensional analytical models (e.g. Mackay, 1972; Lachenbruch et al., 1982) and numerical models (Oucalt, 1985; Nixon, 1986) for the transient response of permafrost to submergence generally suggest the presence of relatively thick subsea permafrost even in areas of deeper water. The occurrence of subsea permafrost implies the potential presence of stability zones for gas hydrates. However, one-dimensional models are not completely satisfactory because of possible lateral heat flow in the subsea permafrost particularly near shore. In some cases, it may also be necessary to include distributed latent heat effects and variable thermal parameters associated with the potential presence of saline pore fluids in the permafrost, which do not appear to have been done.

This paper presents the results of two-dimensional numerical modeling of the thermal response of permafrost to changes in sea level and climate, which includes the effects of saline pore fluids on latent heat and thermal parameters. The region considered was the continental shelf of Alaska near Lonely. Results of these simulations are used to evaluate, at the present time, the spatial distribution of IBP in the continental shelf near Lonely and the stability zones of gas

hydrates that may exist within or under the permafrost.

Additional information on the numerical simulations, study site, choice of parameters, initial conditions, boundary conditions, and other simulations may be found in Fei (1992).

#### STUDY SITE

The study site, offshore from Lonely which is about 135 km southeast of Barrow, Alaska, was chosen because of the availability of data from other research and from onshore and offshore petroleum exploration wells. Available data consist of geophysical logs and samples from the J.W. Dalton-1 (JWD) well onshore and the Antares well offshore (Collett et al., 1989; Deming et al., 1992), results of thermal studies in five shallow drill holes along an offshore line to the northwest from Lonely (Harrison and Osterkamp, 1981), and results of bottom sampling and shoreline erosion studies (Hopkins and Hartz, 1978).

The onshore surficial deposits were mapped as interglacial nearshore and lagoon sand, silty fine sand, and pebbly sand (Hopkins and Hartz, 1978). Shallow offshore drilling data (Harrison and Osterkamp, 1981) indicate that the seabed sediments are fine-grained to about the 30 m depth. At the JWD well, the deeper well logs indicate relatively coarse material (conglomerate and sandstone) down to the 270 m to 300 m depth or so overlying finer material (siltstone) (Collett et al., 1989). There is a change in the temperature gradient in this depth interval (Lachenbruch and Marshall, 1986). We interpret the base of the IBP to be at 360 m to 366 m (about  $-2.2^{\circ}\text{C}$ ) where slight changes in the resistivity log and the temperature gradient occur. Other onshore wells in this region indicate a similar lithology but generally with somewhat finer material.

The nearest offshore well (Antares, EXXON) is about 24 km distant on a line bearing  $\text{N}55^{\circ}\text{E}$  from Lonely in about 15 m of water. Well logs indicate that relatively fine-grained material exists in the upper section (above 190 m) where permafrost might be expected with some coarser material from 190 m to 312 m. The use of geophysical logs to determine the presence or absence of IBP is very difficult because of the lack of contrast in physical properties between the thawed material and any warm and marginally ice-bearing permafrost which would be thawing from both the top and bottom. According to the gamma ray log, there are two similar sections just above 272 m and 305 m. Increases in the resistivity log (DIL) above 272 m but not above 305 m suggest that IBP may exist above 272 m which is our interpretation of the log. However, other factors (e.g., changes in pore fluid salinity) besides permafrost could produce these increases.

The harmonic mean thermal conductivity determined from drill cuttings from the JWD well in the frozen interval from 113 m to 269 m is  $2.57 \text{ W(mK)}^{-1}$  (Deming et al., 1992). Values of  $2.5 \text{ W(mK)}^{-1}$  and  $1.7 \text{ W(mK)}^{-1}$  were used for the frozen and unfrozen material respectively. The porosity was assumed to be 0.2. For fine-grained sediments containing brines, the temperature-dependent thermal parameters were calculated using an unfrozen water content,  $\theta_u = AT^B$ , where  $T$  is the magnitude of the temperature ( $^{\circ}\text{C}$ ) and  $A$  and  $B$  are empirical constants ( $A = 0.1435$ ,  $B = -0.902$ ) (Fei, 1992). Freezing point depression was assumed to be  $-1.63^{\circ}\text{C}$ . The volumetric heat capacity and the thermal diffusivity were calculated according to the methods used by Osterkamp (1987).

Deming et al. (1992) suggest a large heat flow of  $\approx 80 \text{ mW}\cdot\text{m}^{-2}$  for the JWD well. However, the average measured temperature gradient and the above frozen conductivity yield a more normal value of  $\approx 54 \text{ mW}\cdot\text{m}^{-2}$  in the upper interval. For the simulations, a compromise value of  $65 \text{ mW}\cdot\text{m}^{-2}$  was used.

Information on the near surface seabed sediments, temperatures, and depth to IBP was obtained in five shallow drill holes which were rotary jet drilled along a line bearing  $\text{N}32^{\circ}\text{W}$  near the DEW site at Lonely (Harrison and Osterkamp, 1981). Distances from shore were paced and may contain significant errors.

Figure 1 shows temperature profiles measured in these holes, two to three weeks after drilling, which are thought to be within a few hundredths degree of equilibrium values. The profiles show a decreasing thermal gradient with distance (time) offshore. Assuming the current average shoreline erosion rate ( $4.7 \text{ m}\cdot\text{a}^{-1}$ ), the hole at 7770 m offshore has been submerged for about seventeen centuries. Approximate mean seabed temperatures can be obtained by projecting the thermal gradients in the deeper part of the holes up to the seabed. However, the presence of a phase boundary often makes it difficult to do this reliably.

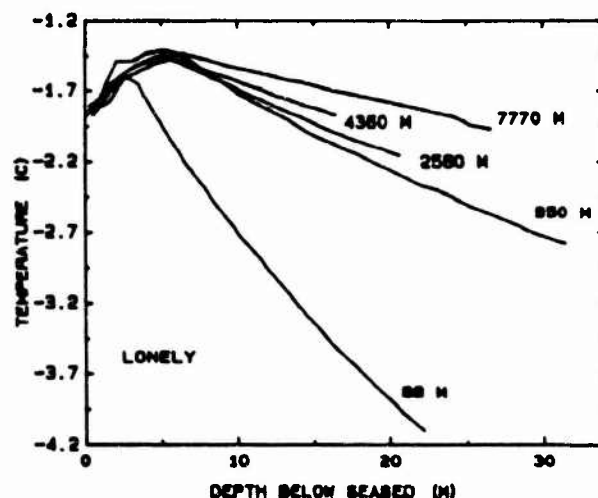


Figure 1. Subsea permafrost temperatures measured in five, shallow, offshore holes along a line bearing  $\text{N}32^{\circ}\text{W}$  at Lonely, Alaska. The numbers next to the profiles are the estimated distances offshore which were paced and may contain significant errors.

In warm subsea permafrost which contains brines, the amount of ice appears to increase gradually with depth (Osterkamp and Harrison, 1982; Osterkamp et al., 1989). Consequently, there is no distinct change in temperature gradient nor properties at the IBP table but only a gradual curvature of the temperature profile which makes it difficult to detect the presence of ice from the drilling data or the temperature data (Fig. 1). Therefore, the holes were heated to determine the presence of ice using the method described by Osterkamp and Harrison (1980). Our interpretation of the results of drilling and heating the holes indicate that the IBP table occurs between 6 m and 15 m below the seabed along this line (Table 1).

Table 1. Data for holes drilled at Lonely along a line N32°W starting at a point on the shoreline which was N66°W from the DEW site radar dome. The hole number is the distance from shore in meters determined by pacing.

Hole Number	Drilling Date	Water Depth	Sea Ice Thickness	Ice-Bearing Permafrost Table	
				Depth	Temperature
88	5/8/80	1.98 m	1.45 m	6-7 m	-2.2°C
950	5/9/80	3.12 m	1.58 m	7-14 m	-1.6 to -1.9°C
2560	5/10/80	4.80 m	1.47 m	8-13 m	-1.6 to -1.9°C
4360	5/11/80	6.50 m	2.1 m (rafted?)	7-12 m	-1.5 to -1.7°C
7770	5/13/80	7.70 m	1.39 m	7-15 m	-1.5 to -1.7°C

Simulations were done for two lines, one bearing N32°W (Table 1) which crosses the shelf at an angle and one bearing N20°E which is perpendicular to the depth contours and passes about 15 km to the west of the Antares well. Seabed profiles for these lines were constructed using results from the above studies and bathymetric maps. Two simulations for the latter line are reported herein, one for sediments with fresh-water pore fluids and one for sediments containing sea water brines. Our strategy was to perform two simulations for two near-extreme cases with regard to their effects on the thermal state of the permafrost. Additional details and simulations are discussed in Fei (1992).

#### INITIAL AND BOUNDARY CONDITIONS

The initial thermal conditions are unknown. However, the simulations were started using steady state conditions (Lachenbruch, 1957) far enough into the past (121 Kyr BP) to allow any transients (Osterkamp and Gosink, 1991) associated with the initial conditions to disappear. The surface boundary condition depends on whether the surface is emergent or submergent. For the emergent surface temperature, the paleoclimatic temperature history of Maximova and Romanovsky (1988), modified for the Lonely region (Osterkamp and Gosink 1991), was used. Their history gives good agreement with the current permafrost thickness at Prudhoe Bay (Osterkamp and Gosink, 1991). Since there does not appear to be a sea level history curve for this portion of the Beaufort Sea shelf, the timing for emergence and submergence was obtained from the sea level history curve of Bard et al. (1990) modified to take shoreline erosion into account (Fei, 1992). This procedure produces depths to the seabed that are somewhat shallower than observed up to 20 km offshore. For the submerged surface, current seabed temperatures determined from measurements in shallow drill holes at Prudhoe Bay, Barrow, and Lonely, adjusted for water depth, were used (Fig. 1 and Osterkamp and Harrison, 1982, 1985). Additional information is provided by Fei (1992).

#### RESULTS AND DISCUSSION

##### Fine-Grained Material Containing Brines

Figure 2 shows the predicted current temperature distribution in the continental shelf along the line bearing N20°E from Lonely. The uneven character of the isotherms in Figure 2 is caused by the plotting algorithm. IBP (-1.6°C isotherm) is predicted to extend only about 19 km offshore. This surprising prediction is a result of the relatively large heat flow and low ice content assumed for the IBP.

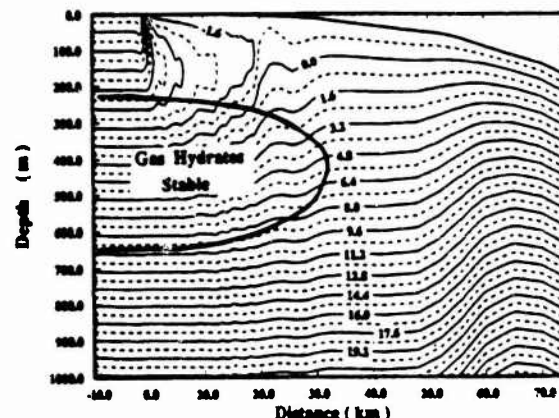


Figure 2. Predicted offshore temperature distribution and stability zone for gas hydrates at the present time near Lonely for fine-grained sediments containing brines. The ice-bearing permafrost is defined by the -1.6°C isotherm.

Lateral heat flow is large in the IBP near the coast, but it is also significant in the rest of the IBP and in the thawed material under it and seaward of it. Beyond 50 km offshore, at deeper depths the curved isotherms and associated lateral heat flow appear to be the result of recently thawed IBP near the seabed. These results suggest that one-dimensional thermal models that assume there is no lateral heat flow may not correctly predict the thermal regime of subsea permafrost containing brines.

The predicted depth to the base of IBP onshore is 318 m compared to the observed depth of 366 m, a difference of 13%. In the offshore region, the base of the IBP rises rapidly with distance offshore. A comparison with the Antares well is difficult since it is about 15 km east of this profile in a water depth of 15 m. If water depth is used as a criterion, this calculated profile predicts an absence of IBP at the Antares well. However, if distance offshore is used, IBP at the Antares well would be predicted to a depth of about 200 m compared to the 272 m observed.

Depth to the IBP table increases almost linearly with distance offshore to about 66 m below the seabed at 19 km offshore. At 7.8 km offshore, the predicted thickness of the thawed layer at the seabed is 21 m. At the same distance offshore, along the line bearing N32°W, the observed thickness is 7 m to 15 m (Table 1). If water depth were used as a criterion, the difference between observed and calculated values would be greater.

### Fine-grained Material with Constant Thermal Properties

Figure 3 shows the predicted current temperature distribution along the line bearing N20°E from Lonely. A nearly isothermal IBP section extends from 4 km to 52 km offshore where the water depth is about 50 m. Up to about 24 km offshore, the IBP section is wedge-shaped and beyond 24 km it is nearly tabular with a relatively flat vertical tip. The relatively thick tabular section appears to be a result of the assumed sea level curve. This curve indicates that depths of less than 50 m were continuously exposed to cold air temperatures for more than 70 kyr and only submerged during the last 11 kyr. This would produce a thick section of IBP out to the current 50 m isobath.

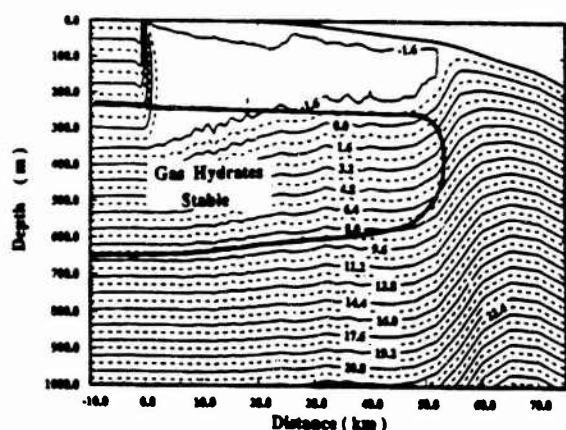


Figure 3. Predicted offshore temperature distribution and stability zone for gas hydrates at the present time near Lonely for fine-grained sediments with constant thermal parameters. The ice-bearing permafrost is defined by the  $-1.6^{\circ}\text{C}$  isotherm.

Lateral heat flow is large within 4 km of shore and in the thawed material beyond and under the tip of the IBP. Predicted depth to the base of the IBP onshore (355 m) is close to the observed value (366 m). This suggests that the full thickness of the IBP may be modeled better with constant thermal properties than with temperature-dependent properties and distributed latent heat effects associated with the presence of brines in the permafrost. A similar result was found by Osterkamp and Gosink (1991) when modeling changes in permafrost thickness at Prudhoe Bay in response to changes in paleoclimate. In the offshore region, the predicted base of the IBP rises rapidly to 24 km offshore and then more slowly farther offshore. Comparison with the Antares well is again difficult. At the equivalent water depth (15 m), the predicted base of the IBP would be at about 210 m below sea level, and at the equivalent distance offshore, about 270 m compared to the observed depth of 272 m.

Depth to the IBP table increases almost linearly with distance offshore and reaches a maximum value of 66 m below the seabed at 22 km offshore. It then rises to within 30 m of the seabed and remains at nearly a constant depth to the tip of the IBP. This behavior is the combined result of the sea level history curve and seabed temperatures. Sea levels rose rapidly from the glacial minimum less than 20 kyr BP to about 4 kyr

BP. As a result, the shelf was rapidly covered with deep cold water (about  $-1.5^{\circ}\text{C}$ ). In the last 4 kyr, submergence (due to sea level rise and shoreline erosion) occurred in shallow warm water (about  $-1^{\circ}\text{C}$ ). In the shallow water, the larger temperature gradient in the thawed material between the seabed and the IBP table ( $-1.63^{\circ}\text{C}$ ) allows for greater heat flow and therefore a faster thawing rate. The predicted thickness of the thawed layer below the seabed is 38m at 7.8 km offshore, much greater than observed along our line of shallow holes (Table 1.). While thawing near the seabed for this case is initially greater than when brines are present, by 19 km offshore the thicknesses of the thawed layers are about equal.

Simulations for both materials were carried out along our line of shallow holes (N32°W) using the above parameters and conditions except for a larger geothermal heat flow of  $80 \text{ mW}\cdot\text{m}^{-2}$  as suggested by Deming et al. (1992). In these cases, predictions for the depth to the base of IBP onshore were much too shallow suggesting that this choice of heat flow may be too large for Lonely.

### Stability Zone for Gas Hydrates

Gas hydrates are stable over a limited range of pressures and temperatures that can be found in association with permafrost, including subsea permafrost (e.g. Kvenvolden and McMenamin, 1980; Collett et al., 1988). The stable region can be determined from the phase equilibrium diagram (Sloan, 1990). It was assumed that the only gas in the hydrate was methane and that pressures could be converted to depth using hydrostatic conditions in the sediments. Latent heat effects due to formation or decay of the gas hydrates were neglected. With these assumptions, the current approximate stability regions for methane gas hydrates in the continental shelf near Lonely were mapped on the two-dimensional depth-temperature diagrams in Fig. 2 and 3.

In fine-grained sediments containing brines, gas hydrates can potentially exist up to 32 km offshore. The stability zone is below 220 m and above 650 m near shore, about the same as that shown in Lachenbruch et al. (1988) for the JWD well. For constant thermal parameters, the depth range of the stability zone near shore is similar; however, the stability zone extends up to about 54 km offshore where the water depth is about 55 m. Using the sea level history curve of Bard et al. (1990), depths of 50 m to 55 m were submerged about  $10^4$  years ago. Thus, the time scale for producing methane gas from destabilized gas hydrates in the continental shelf near Lonely (for constant thermal parameters) is about four times greater than predicted by MacDonald (1990).

### SUMMARY

A two-dimensional finite element model was used to evaluate the thermal response and current thermal regime of permafrost to changes in sea level and climate. This information was used to calculate the current stability zone for gas hydrates in the continental shelf. The study site, offshore from Lonely, was chosen because of the availability of data from other research and from two oil exploration wells, one onshore and one offshore. These data were used to provide information on sediment types, depths to the permafrost table and base, thermal properties of the sediments, heat flow, shoreline erosion rate, and boundary conditions for modeling. Simulations were carried out for two extreme cases, permafrost with constant thermal parameters and permafrost containing sea water brines which introduce distributed latent heat effects and cause the

thermal parameters to have a strong dependence on temperature. These two cases span a wide range of thermal parameters and produce results for the thermal states of the permafrost which are quite different.

For the case when the permafrost contains brines, ice-bearing permafrost (IBP) is predicted to extend only 19 km offshore. This is a result of the relatively large heat flow ( $65 \text{ mW}\cdot\text{m}^{-2}$ ) and low ice content (porosity) assumed for the IBP. Lateral heat flow is significant throughout the IBP and in the thawed material under it and seaward of it. This suggests that one-dimensional thermal models may not correctly predict the thermal regime of subsea permafrost containing brine. Depth to the IBP table increases almost linearly with distance offshore and, at 7.8 km, is 28 m compared to the 7 m to 15 m observed along another line at the same distance offshore.

For the case when thermal properties are constant, IBP is predicted to extend 52 km offshore where the water depth is 50 m. The IBP is primarily isothermal, wedge shaped to 24 km offshore, nearly tabular beyond 24 km offshore, and has a relatively flat vertical tip. Depth to the IBP table increases almost linearly with distance offshore over the wedge shaped section and is relatively shallow and nearly constant over the tabular section. This behavior is the combined result of the assumed sea level history curve and seabed temperatures. At 7.8 km offshore, the predicted thickness of the thawed layer at the seabed is 38 m compared to 7 m to 15 m observed along another line at the same distance offshore.

Predicted depth to the base of IBP onshore obtained by applying the model with constant thermal properties (355 m) is in better agreement with the observed value (366 m) compared to the prediction using temperature-dependent thermal properties (318 m). This suggests that the full thickness of the IBP can be modeled better with constant thermal properties. However, the depth to the IBP table appears to be predicted better using the model where the permafrost contains brines. While thawing of subsea permafrost is a complex process possibly involving convective heat flow by movement of the brines, this suggests that most of the deeper permafrost may be relatively free of brines but that the near-surface permafrost contains brines, although other factors may play a role.

Simulations using the large heat flow ( $80 \text{ mW}\cdot\text{m}^{-2}$ ) suggested by Deming et al. (1992) resulted in predictions for the base of the IBP which were much too shallow.

The predicted zone for stability of methane gas hydrates is below about 220 m and above about 650 m near shore. When the permafrost contains brines, this stability zone extends 32 km offshore. For permafrost with constant thermal properties, the stability zone extends 54 km offshore to the 55 m water depth. Submergence occurred at this water depth about  $10^4$  years ago. This indicates that the time scale for producing methane gas from destabilized gas hydrates in the continental shelf near Lonely is about four times greater than predicted by MacDonald (1990).

#### ACKNOWLEDGMENTS

We wish to thank T.S. Collett and Dr. J.P. Gosink for their comments on this research. The finite element model used for these simulations was developed by Dr. J.P. Gosink. This research was funded by the Army Research Office, National Science Foundation, U.S. Geological Survey and by the State of Alaska.

#### REFERENCES

- Bard, E., B. Hamelin, and R.G. Fairbanks (1990) U-Th ages obtained by mass spectrometry in corals from Barbados: sea level during the past 130,000 years, *Nature*, 346, 456-458.
- Clarke, J.W., P.S. Amand, and M. Matson (1986) Possible cause of plumes from Bennett Island, Soviet Far Arctic, *Bull. Am. Assoc. Pet. Geol.*, 70(5), 574.
- Collett, T.S., K.J. Bird, K.A. Kvenvolden, and L.B. Magoon (1988) Geologic interrelations relative to gas hydrates within the North Slope of Alaska, Open-File Rept. 88-389, USGS, Menlo Park, CA.
- Collett, T.S., K.J. Bird, K.J. Kvenvolden, and L.B. Magoon (1989) Map showing the depth to base of the deepest ice-bearing permafrost as determined from well logs, North Slope, Alaska, U.S.G.S., Oil and Gas Investigations, Map OM-222.
- Deming, D., J.H. Sass, A.H. Lachenbruch, and R.F. DeRito (1992) Heat flow and subsurface temperature as evidence for basin scale groundwater flow, North Slope of Alaska, *GSA Bull.*, 104, 528-542.
- Fei, T. (1992) A theoretical study of the effects of sea level and climatic change on permafrost temperatures and gas hydrates, unpublished M.S. Thesis, 102 pp., Univ. of Alaska, Fairbanks, AK.
- Harrison, W.D., and T.E. Osterkamp (1981) Subsea permafrost: probing, thermal regime, and data analyses, Annual Rept. to NOAA, ERL, Boulder, CO.
- Hopkins, D.M., and R.W. Hartz (1978) Shoreline history of Chukchi and Beaufort Seas as an aid to predicting offshore permafrost conditions, *Environmental Assessment of the Alaskan Continental Shelf*, Annual Rept., 12, 503-575.
- Hunter, J.A.M., A.S. Judge, H.A. MacAulay, R.L. Good, R. M. Gagne, and R.A. Burns (1976) Permafrost and frozen sub-seabottom materials in the Southern Beaufort Sea, Tech. Rept. 22, Beaufort Sea Project, Dept. of the Environment, Victoria, B.C.
- Kvenvolden, K.A., and M.A. McMenamin (1980) Hydrates of natural gas: A review of their geological occurrence, USGS Circular 825, Arlington, VA.
- Lachenbruch, A.H. (1957) Thermal effects of the ocean on permafrost, *GSA Bull.*, 68, 1515-1530.
- Lachenbruch, A.H., J. H. Sass, B.V. Marshall, and T. H. Moses Jr. (1982) Permafrost, heat flow, and the geothermal regime at Prudhoe Bay, Alaska, *J. Geophys. Res.*, 87 (B11), 9301-9316.
- Lachenbruch, A.H., and B.V. Marshall (1986) Changing climate: geothermal evidence from permafrost in the Alaskan Arctic, *Science*, 234, 689-696.
- Lachenbruch, A.H. and others (1988) Temperature and depth of permafrost on the Arctic Slope of Alaska, in U.S.G.S. Prof. Paper 1399, p. 645-656.
- Lewellen, R.I. (1973) The occurrence and characteristics of nearshore permafrost, Northern Alaska, *Proc. Second Int. Conf. on Permafrost*, 131-135, NAS, Washington, D.C.
- MacDonald, G.J. (1990) Role of methane clathrates in past and future climates, *Climatic Change*, 16, 247-281.
- Mackay, J.R. (1972) Offshore permafrost and ground ice, Southern Beaufort Sea, Canada, *Can. J. Earth Sci.*, 9(11), 1550-1561.
- Maximova, L.N., and V.E. Romanovsky (1988) A hypothesis for the Holocene permafrost evolution, *Proc. of the Fifth Int. Conf. on Permafrost*, 1, 102-106, Norwegian Inst. of Tech., Trondheim, Norway.

- Molochushkin, E.N. (1978) The effect of thermal abrasion on the temperature of the permafrost in the coastal zone of the Laptev Sea, p. 90-93, USSR Contribution, Permafrost, Second Int. Conf., July 13-28, 1973, NAS, Washington, D.C.
- Nixon, J.F. (1986) Thermal simulation of subsea permafrost, *Can. J. Earth Sci.*, 23, 2039-2046.
- Osterkamp, T.E. (1987) Freezing and thawing of soils and permafrost containing unfrozen water or brine, *Water Resources Res.*, 23(12), 2279-2285.
- Osterkamp, T.E., and W.D. Harrison (1980) Subsea permafrost: probing, thermal regime, and data analyses, Annual Rept. to NOAA, ERL, Boulder, CO.
- Osterkamp, T.E., and W.D. Harrison (1982) Temperature measurements in subsea permafrost off the coast of Alaska, *Proc. Fourth Canadian Permafrost Conf.*, pp. 238-248, National Research Council of Canada, Ottawa, Canada.
- Osterkamp, T.E., and W.D. Harrison (1985) Subsea permafrost: probing, thermal regime, and data analyses, 1975-1981, Rept. UAGR301, 108 pp., Geophys. Inst., Univ. of Alaska, Fairbanks, AK.
- Osterkamp, T.E., J.K. Petersen, and T.S. Collett (1985) Permafrost thicknesses in the Oliktok Point, Prudhoe Bay, and Mikkelson bay areas of Alaska, *Cold Reg. Sci. and Eng.*, 11, 99-105.
- Osterkamp, T.E., G.C. Baker, W.D. Harrison, and T. Matava (1989) Characteristics of the active layer and subsea permafrost, *J. Geophys. Res.*, 94(C11), 16,227-16,236.
- Osterkamp, T.E., and J.P. Gosink (1991) Variations in permafrost thickness in response to changes in paleoclimate, *J. Geophys. Res.*, 96(B3), 4423-4434.
- Outcalt, S. (1985) A numerical model of subsea permafrost in freezing and thawing of soil-water systems, TCCRE Monograph, D.M. Anderson and P.J. Williams, eds., ASCE, New York, NY.
- Shackleton, N.J., and N.D. Opdyke (1977) Oxygen isotope and paleomagnetic evidence for early northern hemisphere glaciation, *Nature*, 270, 216-219.
- Sloan, E.D., Jr. (1990) Clathrate hydrates of natural gases, 641 pp., Marcel Dekker, Inc., New York, NY.

## Modeling the Response of Permafrost and Gas Hydrates to Changes in Sea Level and Climate

T. E. Osterkamp and T. Fei (Both at: Geophysical Institute, University of Alaska Fairbanks, Fairbanks, AK 99775-0800; 907-474-7548)

A two-dimensional finite element model was used to investigate the thermal response of subsea permafrost and gas hydrates to changes in sea level and climate along a line offshore from Lonely, Alaska. Simulations were carried out for two extreme cases: permafrost with constant thermal parameters; and, permafrost with temperature-dependent thermal parameters and distributed latent heat effects due to the presence of brines. For subsea permafrost containing brines, the ice-bearing permafrost (IBP) is predicted to be wedge shaped and to extend only 19 km offshore. There is significant lateral heat flow throughout the IBP section and the depth to the IBP table increases almost linearly with distance offshore. For subsea permafrost with constant thermal parameters, IBP is predicted to extend 52 km offshore (water depth ~ 50 m) and is nearly isothermal beyond 4 km offshore. It is wedge shaped up to 24 km offshore, tabular beyond, and has a flat vertical tip. Depth to the IBP increases almost linearly with distance offshore over the wedge-shaped section and is relatively shallow and nearly constant over the tabular section. Seabed temperatures and the assumed sea level history curve are especially important in determining the current distribution of subsea permafrost. The full thickness of IBP onshore can be modeled better with constant thermal parameters compared to permafrost that contains brines. Depth to the IBP table offshore may be modeled better when it is assumed that the permafrost contains brines. The predicted zone for stability of methane gas hydrates is between 220 m and 650 m near shore. For subsea permafrost containing brines, this zone extends 32 km offshore compared to 54 km (to the 55 m water depth) for constant thermal parameters. The time scale for producing methane gas from destabilized gas hydrates in the continental shelf near Lonely is on the order of  $10^4$  years, much longer than previously predicted.

## **Modeling the Response of Permafrost to Surface Temperature Changes in the Alaskan Arctic**

**T. Zhang and T. E. Osterkamp** (Both at: Geophysical Institute, University of Alaska Fairbanks, Fairbanks, AK 99775-0800; 907-474-7548)

Climatological data and modeling have been used to investigate the response of permafrost in the Alaskan Arctic north of the Brooks Range to changes in climate over the last century or so. Air temperatures in this region are strongly correlated, vary with periods of 10 years and 47 years, and follow the same general trends as the North American Arctic. Precipitation, primarily snowfall, which was heavier during cold periods and lighter during warm periods, was poorly correlated between stations, and showed a periodicity of 37 years at Barrow and 34 years at Barter Island. These results suggest that the effects of changes in air temperatures on permafrost temperatures may have been modified by changes in snow cover. A numerical model using North American Arctic air temperatures at the permafrost surface showed that the permafrost temperature variations depended strongly on the choice of initial conditions, that air temperature changes were sufficiently large to account for the observations, and that air temperature changes predated permafrost temperature changes. An alternative explanation of the last result is that the shallow permafrost temperatures were colder than the assumed initial conditions. The model with Barrow air temperatures (1923-1991) applied at the ground surface with no snow cover predicted a slight cooling of permafrost temperatures at present. Adding the snow cover caused the permafrost to warm with about the same magnitude and penetration depth as observed. The results may explain why different sites show a warming, little or no change, or a cooling of permafrost temperatures. Current interpretations of observed permafrost temperature changes are unsatisfactory. The data indicate that the warming at most sites occurred just before or later than 1920. However, air temperature trends from about 1920 to present appear to have been within a degree or so of the long-term mean at Barrow ( $-12.5^{\circ}\text{C}$ ). It is difficult to see how air temperature changes alone could have produced the observed warming at Prudhoe Bay ( $2^{\circ}\text{C}$  to  $3^{\circ}\text{C}$ ). Current differences between air and permafrost temperatures are about  $3^{\circ}\text{C}$  to  $6^{\circ}\text{C}$ . If an equilibrium initial condition is assumed for the permafrost in 1923, then this difference must have been on the order of a degree or less. This implies a very thin snow cover prior to that time, non-equilibrium conditions in 1880, or some other unknown factor. Variations in snowfall may be largely responsible for the observed warming of permafrost temperatures; however, there is insufficient long-term data to directly test this hypothesis.

# Considerations in Determining Thermal Diffusivity from Temperature Time Series Using Numerical Methods

T. Zhang and T. E. Osterkamp

*Geophysical Institute, University of Alaska Fairbanks, 99775-0800*

## ABSTRACT

This paper investigates numerical methods for determining the in situ apparent thermal diffusivity,  $D$ , of the active layer and permafrost from repeated measurements of vertical temperature profiles. The results can be applied to any soil or rock where heat flow is conductive. An analytical expression was derived for  $D$  when unfrozen water is present in frozen soils and permafrost. The usual numerical expression for  $D$  (termed model I) was extended to include higher order terms (model II). This substantially reduces truncation errors but increases measurement errors somewhat. Extremely accurate temperature measurements (approaching  $\pm 0.01^\circ\text{C}$ ) are required to apply the method. Synthetic temperature time series were used to evaluate and compare predictions of models I and II. Model I produced spikes (large positive and negative values) in the calculated  $D$  at times where the ground temperatures were near a maximum or minimum. Using model II, the spikes disappeared or were substantially reduced in magnitude and duration and errors in  $D$  at other times were reduced compared to model I. Application of the method requires acquisition of very precise temperature measurements at appropriate space ( $\Delta x$ ) and time ( $\Delta t$ ) intervals at a depth where measurable temperature changes occur. Selection of values for  $\Delta x$  and  $\Delta t$  must take into account the accuracy of the temperature measurements, duration and amplitude of the temperature changes, depth, and the expected values for  $D$ . In general,  $\Delta x$  should be much less than the depth of interest and  $\Delta t$  must be less than the period or duration of surface temperature changes. For the active layer,  $\Delta x$  can range from a few centimeters to a tenth of a meter or so and  $\Delta t$  from a few minutes to an hour or so. For the near-surface permafrost within the depth of annual temperature variations,  $\Delta x$  can range from a few tenths of a meter to about one meter and  $\Delta t$  from one day to several weeks. Below the depth of annual temperature variations in the permafrost, values for  $\Delta x$  of several meters and  $\Delta t$  of a year or more may be appropriate.

## INTRODUCTION

Investigations of the thermal regime of the active layer and permafrost require an understanding of their thermal properties, particularly thermal conductivity, volumetric heat capacity and thermal diffusivity. The thermal diffusivity is of primary importance in natural systems since it controls the rate of thermal response. McGaw *et al.*, (1978) developed a method to determine thermal diffusivity *in situ* for the active layer and permafrost from a temperature time series. This method has also been used by Nelson *et al.* (1985), Outcalt and Hinkel (1989, 1990), Zhang (1989), and Hinkel *et al.* (1990). While it appears that good results can be obtained, reported *in situ* values for thermal diffusivity are sometimes large, contain zero values, may be negative, and have considerable scatter. Using a synthetic thermal profile, Hinkel *et al.* (1990) showed that large positive and negative values ("spikes") were a result of the method and occur when the rate of change of the temperature gradient becomes small. They attributed other large fluctuations in thermal diffusivity to non-conductive heat flow processes in the active layer; a conclusion which is rendered uncertain by the variable results for D.

This paper investigates further the application of numerical methods for determining the thermal diffusivity of the active layer and permafrost from temperature time series.

## REVIEW OF THEORY

The one-dimensional transient heat conduction equation is

$$\frac{\partial}{\partial x} \left( K \frac{\partial T}{\partial x} \right) = C_v \frac{\partial T}{\partial t} \quad (1)$$

where  $K$  is the thermal conductivity ( $Wm^{-1}^{\circ}C^{-1}$ ),  $T$  is the temperature ( $^{\circ}C$ ),  $x$  is the distance coordinate (m),  $C_v$  is the volumetric heat capacity ( $Jm^{-3}^{\circ}C^{-1}$ ) and  $t$  is the time (sec).

In the application of (1), it is often assumed that  $K$  does not depend on position (i.e., the soil is homogeneous). In a thawed active layer and in a frozen active layer and permafrost that does not contain unfrozen water,  $K$  and  $C_v$  are approximately independent of temperature. With these assumptions, (1) becomes

$$\frac{\partial^2 T}{\partial x^2} = \frac{1}{D} \frac{\partial T}{\partial t} \quad (2)$$

where  $D = K/C_v$  is the thermal diffusivity ( $m^2/sec$ ).

Equation (2) has been used in the past to calculate an apparent thermal diffusivity  $D = T_t/T_{xx}$ , where  $T_t$  and  $T_{xx}$  are the numerical approximations of  $\partial T/\partial t$  and  $\partial^2 T/\partial x^2$ , respectively. This relation has a singular point at  $T_{xx} = 0$  which may create difficulties when using it to calculate  $D$ .

If the active layer and permafrost are partially frozen and contain unfrozen water, then  $K$  and  $C_v$  are functions of temperature. Equation (1) becomes (Guymon, 1984)

$$K \frac{\partial^2 T}{\partial x^2} + \frac{\partial K}{\partial T} \left( \frac{\partial T}{\partial x} \right)^2 = C_v \frac{\partial T}{\partial t} - L \frac{\rho_i}{\rho_u} \frac{\partial \theta_i}{\partial t} \quad (3)$$

where  $L$  is the volumetric latent heat of fusion ( $Jm^{-3}$ ),  $\theta_i$  is the volumetric ice content ( $m^3/m^3$ ), and  $\rho_i$  and  $\rho_u$  are the densities of ice and unfrozen water, respectively. Equation (3) can be written

$$K \frac{\partial^2 T}{\partial x^2} + \frac{\partial K}{\partial T} \left( \frac{\partial T}{\partial x} \right)^2 = C_a \frac{\partial T}{\partial t} \quad (4)$$

where  $C_a = C_v + L(\partial \theta_u / \partial T)$  is the apparent volumetric heat capacity and  $\theta_u$  is the volumetric unfrozen water content ( $m^3/m^3$ ) (eg. Osterkamp, 1987). An apparent thermal diffusivity for frozen soils and permafrost containing unfrozen water can be defined as follows. For saturated soils, common in permafrost and the active layer,

$$K = K_s^{(1-\theta_f)} K_i^{\theta_f} \left( \frac{K_u}{K_i} \right)^{\theta_u} \quad (5)$$

where  $K_s$ ,  $K_i$  and  $K_u$  are the thermal conductivities of the soil, ice and unfrozen water components, and  $\theta_f$  is the porosity in the frozen state. The temperature dependence of the thermal conductivity of the constituents is ignored over the range of temperatures usually found in the field. Using  $\theta_u = \rho_b w_u / \rho_u$  and  $w_u = A(-T)^B$ , where  $\rho_b$  is the bulk density of the soil ( $kg/m^3$ ),  $\rho_u$  is the density of unfrozen water,  $w_u$  is the gravimetric water content ( $kg/kg$ ), and  $A$  and  $B$  are constants, then

$$\frac{1}{K} \frac{\partial K}{\partial T} = -R(-T)^{B-1} \quad (6)$$

where  $R = AB\rho_b \ln(K_u/K_i)/\rho_u$ . Then, (4) becomes

$$D \left[ \frac{\partial^2 T}{\partial x^2} - R(-T)^{B-1} \left( \frac{\partial T}{\partial x} \right)^2 \right] = \frac{\partial T}{\partial t} \quad (7)$$

and

$$D = \frac{T_t}{T_{xx} - RT_x^2(-T)^{B-1}} \quad (8)$$

where  $T_x$  is  $\partial T / \partial x$ . Application of (8) requires a knowledge of the variation of  $\theta_u$  and  $R$  with temperature.

If the water in the thawed active layer or the unfrozen water in the partially frozen active layer or permafrost moves with a constant velocity,  $v$ , then a term of the form  $C_w v \partial T / \partial x$  (e.g., Guymon, 1984), where  $C_w$  is the volumetric heat capacity of water, would be subtracted from the left hand side of (4). This term, divided by  $C_a$ , would then enter into the numerator on the right hand side of (8) and then both  $v$  and  $C_a$  have to be known in order to evaluate  $D$ . Until present, only (2) has been used to evaluate  $D$ ; however, when unfrozen water is present,  $K$  and  $C_a$  are strongly dependent on  $\theta_u$  and (8) is more suitable.

The application of (2) for evaluating  $D$  requires computation of  $T_t$  and  $T_{xx}$  by numerical methods. Two models will be discussed.

**Model I** The numerical approximations of the derivatives  $T_t$  and  $T_{xx}$  are (Gerald and Wheatley, 1989)

$$T_t = \frac{T_i^{j+1} - T_i^{j-1}}{2\Delta t} + O[(\Delta t)^2] \quad (9)$$

and

$$T_{xx} = \frac{T_{i-1}^j - 2T_i^j + T_{i+1}^j}{(\Delta x)^2} + O[(\Delta x)^2] \quad (10)$$

where the integers  $i$  and  $j$  reference positions and times for the node of interest and  $\Delta x$  and  $\Delta t$  represent increments of depth and time in the observation mesh. Equation (9) can also be approximated by (Carnahan et. al., 1969)

$$T_t' = \frac{T_i^{j+1} - T_i^j}{\Delta t} + O[(\Delta t)]. \quad (11)$$

Equations (9) and (11) are alternate expressions which can be used for numerical calculations where (9) involves two time steps and (11) involves only one time step.

Let  $\Delta_t T = T_i^{j+1} - T_i^{j-1}$ ,  $\Delta_{xx} T = T_{i-1}^j - 2T_i^j + T_{i+1}^j$  and  $\Delta_t T' = T_i^{j+1} - T_i^j$ , then, neglecting the terms  $O[(\Delta x)^2]$  and  $O[(\Delta t)^2]$ , substituting (9) and (10) into (2) and rearranging yields

$$D \cong \left( \frac{(\Delta x)^2}{2\Delta t} \right) \frac{\Delta_t T}{\Delta_{xx} T}. \quad (12)$$

Similarly, substituting (10) and (11) into (2) yields

$$D \cong \left( \frac{(\Delta x)^2}{\Delta t} \right) \frac{\Delta_t T'}{\Delta_{xx} T}. \quad (13)$$

The application of (12) requires three temperature profiles with two time steps and (13) requires two temperature profiles with only one time step. Equation (12) has been used by McGaw, et al. (1978); Nelson, et al. (1985); Zhang (1989); Hinkel, et al. (1990) and (13) by Zhang (1989) to compute the apparent thermal diffusivity in the active layer and permafrost.

**Model II** Numerical approximations (truncation errors) of derivatives can be improved by retaining higher order terms in the interpolating polynomial (Gerald and Wheatley, 1989). A Taylor series expansion with higher order terms was used to obtain

$$T_t = \frac{1}{12\Delta t} (T_i^{j-2} - 8T_i^{j-1} + 8T_i^{j+1} - T_i^{j+2}) + O[(\Delta t)^4] \quad (14)$$

and

$$T_{xx} = \frac{1}{12(\Delta x)^2} (-T_{i-2}^j + 16T_{i-1}^j - 30T_i^j + 16T_{i+1}^j - T_{i+2}^j) + O[(\Delta x)^4] \quad (15)$$

Let  $\Delta'_t T = T_i^{j-2} - 8T_i^{j-1} + 8T_i^{j+1} - T_i^{j+2}$  and  $\Delta'_{xx} T = -T_{i-2}^j + 16T_{i-1}^j - 30T_i^j + 16T_{i+1}^j - T_{i+2}^j$ , then, neglecting higher order terms and substituting (14) and (15) into (2),

$$D \cong \left( \frac{(\Delta x)^2}{\Delta t} \right) \frac{\Delta'_t T}{\Delta'_{xx} T}. \quad (16)$$

While application of (16) requires five temperature profiles with four time steps, it should yield a more accurate estimate of  $D$ .

In addition to the obvious requirement that the heat flow must be conductive, there are several general considerations for applying (12), (13), or (16) to field data. First, the heat conduction equation has been derived from continuum theory (Carslaw and Jaeger, 1959) and is valid for an infinitesimally small volume or layer with conductive heat flow while (12), (13), and (16) are for a finite volume. More accurate results using these numerical equations may be expected when  $\Delta x$  and  $\Delta t$  are small; however, both  $\Delta x$  and  $\Delta t$  are restricted by requirements associated with the measuring apparatus. Second, the soil volume in the active layer must be in either a frozen or a thawed state for the time steps of the calculations and the soil volume should be homogeneous. Third, interpolation errors in the numerical procedure depend upon the degree of the polynomial used to obtain the derivatives so that (16) may be expected to give more accurate results than (12) which is more accurate than (13). Round off errors increase as  $\Delta x$  and  $\Delta t$  are decreased since this requires adding and subtracting temperatures that are more nearly the same value. Generally, round off errors can be reduced by using double precision (Gerald and Wheatley, 1989). Fourth, the accuracy of the field temperature measurements influences the estimate of  $D$ . The estimate of  $\Delta_t T$ ,  $\Delta'_t T$  and  $\Delta''_t T$  are nearly independent of temperature accuracy, since only the temperature change at one sensor is required, while the estimate of  $\Delta_{xx} T$  and  $\Delta'_{xx} T$  depends upon the accuracy of the sensors. The quantities  $\Delta_{xx} T$  and  $\Delta'_{xx} T$  at any depth should be greater (preferably much greater) than errors,  $\delta(\Delta_{xx} T)$  and  $\delta(\Delta'_{xx} T)$ , in their determination. Thus, temperature variations at depth should be sufficient to make  $\Delta_{xx} T \gg \delta(\Delta_{xx} T)$  or  $\Delta'_{xx} T \gg \delta(\Delta'_{xx} T)$ . Table 1 shows  $\delta(\Delta_{xx} T)$  and  $\delta(\Delta'_{xx} T)$  for errors,  $\delta T$ , in the temperature measurements.

Table 1: Effects of errors,  $\delta T$ , in temperature measurements on  $\delta(\Delta_{xx} T)$  and  $\delta(\Delta'_{xx} T)$  ( $^{\circ}C$ )

$\delta T$	0.2	0.1	0.05	0.02	0.01
$\delta(\Delta_{xx} T)$	0.5	0.3	0.13	0.05	0.03
$\delta(\Delta'_{xx} T)$	7.5	3.8	1.88	0.75	0.38

Since model II uses higher order terms to calculate the derivatives in the expression for  $D$ , it would appear to be superior to model I. An error analysis based upon the accuracy of the temperature measurements required to evaluate (12) and (16) (Table 2) shows that model I produces somewhat more accurate values for  $D$ . For the conditions

in Table 2, the accuracy of the temperature measurements must approach  $\pm 0.01^\circ\text{C}$  or better to obtain reasonable estimates of  $D$ . Considering the increased complexity and reduced accuracy of model II, because of measurement errors, it may not seem worthwhile to use it. However, the reduction in truncation errors for  $T_i$  and  $T_{xx}$  in model II is a much greater factor than the measurement errors which ultimately makes model II much more precise than model I. It will also be shown that the use of model II helps to clarify the interpretation of results obtained with model I. In addition, model II can be used in some cases when model I becomes unstable and produces spikes in the values for  $D$ .

Table 2: Measurement errors in calculated values of  $D$  using models I and II at a depth of 0.3 m for a daily temperature wave with a surface amplitude of  $4^\circ\text{C}$  with  $\Delta x = 0.1\text{ m}$  and  $\Delta t = 10\text{ min}$ .

Temperature accuracy ( $^\circ\text{C}$ )	Model I Error in $D$ ( $\text{m}^2/\text{yr}$ )	Model II Error in $D$ ( $\text{m}^2/\text{yr}$ )
0.1	78	105
0.05	39	52.5
0.01	7.9	10.5
0.001	0.9	1.2

Synthetic temperature time series were calculated for surface temperatures consisting of daily waves, annual waves with a superimposed daily variation and annual waves with a superimposed multi-year linear trend. Wave parameters were chosen to prevent the possibility of phase change. An input value of  $D=25\text{ m}^2\text{ yr}^{-1}$  was used in all of these calculations. Calculated values of  $D$  from these synthetic temperature profiles, using model I (Eq. 12) and model II, were then compared to the input value of  $D$ . The stated errors are the differences between the calculated and input values divided by the input values (percent difference). The results help to illustrate the general considerations noted above and suggest additional factors that should be taken into account when calculating  $D$  from a measured temperature time series.

## RESULTS AND DISCUSSION

### Daily Surface Temperature Variations

Under stable weather conditions, the ground surface is subjected to a daily cycle

of warming and cooling, which can cause measurable temperature changes to depths of about one to two meters. However, the presence of a thaw or a freeze front shields the underlying ground from these changes. Daily temperature variations can be used to determine  $D$  in a thawed or frozen active layer and in the permafrost underlying a frozen active layer. Synthetic temperatures for the daily cycle of warming and cooling were generated with a ground surface temperature

$$T(0, t) = T_d + A_d \cos(\omega_d t) \quad (17)$$

where  $T_d$  is the mean daily surface temperature,  $A_d$  is the amplitude of the daily surface temperature,  $\omega_d = 2\pi/P_d$ , and the period,  $P_d = 1$  day. It was assumed that  $T_d = -10^\circ\text{C}$  and  $A_d = 4^\circ\text{C}$ . Temperatures were generated at 0.1 m increments from the surface to the 0.5 m depth at 10 minute intervals using the steady-state solution of (2) (Carslaw and Jaeger, 1959). Figure 1 shows temperature variations at depths of 0.2 m, 0.3 m and 0.4 m, the variations in  $\Delta_t T$  and  $\Delta_{xx} T$ , and the calculated values (using models I and II) for  $D$  at the 0.3 m depth with  $\Delta t = 10$  minutes. For model I, the calculations were made using the temperatures at 0.2 m, 0.3 m and 0.4 m depths, while for model II the temperatures from 0.1 m to 0.5 m were used.

Figure 1(C) shows that there are significant errors in values for  $D$  calculated with model I. The largest errors occur near times when the temperature vs. time curve at the 0.3 m depth passes through a maximum or minimum (i.e., when the magnitude of  $\Delta_t T$  and  $\Delta_{xx} T$  become small). Large positive and negative spikes in  $D$  are produced at these times. The best agreement of  $D$  with the input value occurs (near) where the magnitudes of  $\Delta_t T$  and  $\Delta_{xx} T$  are largest. Calculations of  $D$  at other depths show that the spikes in  $D$  change with depth and time due to the time lag as the temperature wave penetrates into the ground from the surface.

The results of calculations using model II (Fig. 1C) are much improved over those of model I. Spikes have been eliminated and the maximum error is only 4%. This reduction in error appears to be due to the more accurate higher order approximations (smaller truncation errors) for the derivatives in (2). Results for calculations using double precision (sixteen significant figures) were almost identical to calculations using single precision suggesting that round off errors were small for both models I and II for the conditions of these calculations. Practical disadvantages of model II are that more data are required and these data need to be very accurate.

Figure 2 shows some of the effects of truncation errors in  $D$  when models I and

II are used with different choices for  $\Delta x$  and  $\Delta t$ . In Fig. 2B and 2C,  $\Delta t$  is constant (1 min) and  $\Delta x$  changes from 0.1 m to 0.01 m. For model I, the errors in D decrease at all times for this change in  $\Delta x$  including a decrease in the magnitude and duration of the spikes. In Fig. 2A and 2C,  $\Delta x$  is constant (0.01 m) and  $\Delta t$  changes from 10 min to 1 min. Errors in D for this change in  $\Delta t$  decrease as  $\Delta t$  decreases except at spikes. The duration of the spikes is the same while their magnitude increases as  $\Delta t$  decreases. The results for model II are similar but the errors in D are much smaller (see Fig. 2B) and the spikes are almost eliminated. Since the conditions were the same for both models, this suggests that the above errors are primarily truncation errors in  $\Delta_t T$  and  $\Delta_{xx} T$ .

### Daily and Seasonal Surface Temperature Variations

The ground surface temperature also varies with changes in the weather and seasonal changes over the year. These changes provide an opportunity to obtain D from depths of about 1 m to 20 m or more. However, daily surface temperature variations are superimposed on these changes and must be considered in the methodology. An annual wave with a superimposed daily wave was used to investigate this problem. Synthetic temperature profiles were generated using

$$T(0, t) = T_y + A_d \cos(\omega_d t) + A_y \cos(\omega_y t) \quad (18)$$

where  $T_y$  is the mean annual temperature. The second term on the right hand side of (18) is the daily surface temperature wave and the third is the annual surface wave with amplitude,  $A_y$ , and  $\omega_y = 2\pi/P_y$  where  $P_y = 1$  year.

Several sets of calculations of D were made using (18) with  $A_d$  ranging from  $0^\circ\text{C}$  to  $4^\circ\text{C}$  and  $\Delta t$  from 10 min to 1 day with  $A_y = 16^\circ\text{C}$ ,  $T_y = -20^\circ\text{C}$ , and  $\Delta x = 0.1$  m. For both models I and II at depths up to 1.2 m where daily temperature variations are significant, using  $\Delta t = 1$  day, errors in D were generally large (10 - 30%) and depended on  $A_d$ . Using  $\Delta t = 10$  min, for depths up to 0.5 m, the errors in D for both models were similar, as expected, to those shown in Fig. 1C. These results illustrate the requirement at these shallow depths that  $\Delta t$  must be much smaller than the period,  $P_d$ , and show that the effect of the annual temperature wave on D is not significant.

Using model I at a depth of 0.8 m with  $\Delta t = 1$  hour, the errors in D were small except near the maximum and minimum temperatures at this depth where multiple spikes were produced. These spikes are a result of daily temperature variations which

cause both  $\Delta_{xx}T$  and  $\Delta_t T$  to oscillate with a frequency of one day. The amplitude of the oscillations is such that both  $\Delta_{xx}T$  and  $\Delta_t T$  repeatedly pass through zero values which produces positive and negative spikes in values for  $D$ . Both the magnitude and duration of the spikes were reduced when using model II.

Values for  $D$  were calculated using models I and II for depths from 4 m to 20 m with  $A_d = 4^\circ C$ ,  $A_y = 16^\circ C$ ,  $T_y = -20^\circ C$ ,  $\Delta x = 1$  m and  $\Delta t = 5$  days (Fig. 3). For model I, the maximum percent difference between the calculated values and the input value in Fig. 3 was less than 20%. Diffusivity values calculated by model II were almost identical to the input value. Additional calculations show that  $D$  can be obtained in the depth range from 1 m to 20 m or more with  $\Delta x$  ranging from a few tenths of a meter to a few meters and  $\Delta t$  from one day to a few weeks, depending upon the depth of interest.

### Climatic Fluctuations and Ground Surface Temperature Variations

Fluctuations in climate on a scale of years produce changes in air temperatures and in snow cover which can affect permafrost temperatures. These effects can be monitored at depths below the seasonal changes by measuring the temperatures in a drill hole over several years. While the temperature changes at these depths are small, they can usually be measured with precision equipment, and  $D$  can be estimated using temperature recording frequencies from a few months to several years. The method is illustrated using the surface temperature

$$T(0, t) = T_y + A_y \cos(\omega_y t) + C_o t \quad (19)$$

where the initial mean ground surface temperature  $T_y = -20^\circ C$ . The second term on the right side of (19) is the annual temperature wave and the third term is an assumed linear temperature trend at the surface, where  $C_o$  is the rate of temperature change at  $x = 0$ . The initial condition is  $T(x, 0) = T_y + G_o x$ , where the temperature gradient  $G_o = 0.019^\circ C/m$ .

Temperature profiles after 10 years were generated with  $A_y = 16^\circ C$ ,  $C_o = 0.2^\circ C/yr^{-1}$ , for 1 m space and 1 year time intervals. Figure 4 shows the calculated temperature profiles and values for  $D$  predicted by models I and II with  $\Delta x = 4$  m and  $\Delta t = 1$  year. The errors in  $D$  below 35 m were less than 2%. The relatively large errors above 35 m were caused by the annual temperature variations and can be eliminated by choosing  $\Delta t \ll 1$  year. At about 64 m, round off errors begin to affect

the results for both models. Additional calculations show that relatively good results can be obtained for  $\Delta t$  ranging from less than a year to several years.

## APPLICATIONS

The above methodology suggests that it should be possible to obtain values for the thermal diffusivity from a temperature time series, not only in the active layer and near-surface permafrost, but to any depth where there are measurable temperature changes. However, the above results are largely based on assumed periodic surface temperature variations with fixed amplitudes in soil where there is no freezing or thawing. Additional opportunities for determining  $D$  are created by weather patterns and by the presence of a freezing or thawing front in the active layer. For example, Climate in Alaska and other permafrost areas is often dominated by aperiodic temperature fluctuations with varying amplitudes lasting from a few days to a few weeks. Solar radiation at these high latitudes exhibits strong seasonal variations. A seasonal snow cover attenuates air temperature variations reducing the variations in ground surface temperatures. A freezing or thawing front in the active layer shields the underlying active layer and permafrost from ground surface temperature variations since the temperature at a front is generally constrained by the requirement for phase equilibrium to be near  $0^{\circ}\text{C}$ . As the ground surface warms and the active layer begins to thaw, the remaining frozen active layer and permafrost warm slowly with time. As the ground surface cools and begins to freeze, the remaining thawed active layer becomes isothermal since it is bounded on the top by the freezing front and on the bottom by the permafrost table. Upward freezing at the base of the active layer causes the adjacent permafrost to cool while the deeper permafrost continues to warm. The temperature changes brought about by these thawing and freezing effects generally continue for about six to nine months each year.

Applications of the method require the acquisition of very precise temperature data (preferably  $\pm 0.01^{\circ}\text{C}$  or better) at appropriate depth ( $\Delta x$ ) and time ( $\Delta t$ ) intervals. Selection of values for  $\Delta x$  and  $\Delta t$  must take into account the accuracy of the temperature measurements, duration and amplitude of the temperature changes, depth where  $D$  is to be determined, and the diffusivity of the soil. Since the diffusivity of the soil can easily vary from 10 to  $50\text{ m}^2\text{ yr}^{-1}$ , a factor of five or more, it is desirable to have information which allows a rough initial estimate of  $D$  to be made. A periodic surface temperature wave can be helpful in making initial estimates for  $\Delta x$  and  $\Delta t$  provided some information is available on the wave parameters. For a periodic surface temperature variation with surface amplitude,  $A$ , and frequency,  $\omega$ , the depth,  $X$ ,

where the amplitude of the temperature variation is  $A_z$  can be obtained from (Carslaw and Jaeger, 1959)

$$X = \ln\left(\frac{A}{A_z}\right) / \sqrt{\frac{\omega}{2D}} \quad (20)$$

Table 3 gives the depths for a daily temperature wave ( $X_d$ ) and an annual wave ( $X_y$ ) where the amplitude has been reduced to  $A_z$  for  $D = 25 \text{ m}^2 \text{ yr}^{-1}$ ,  $A_d = 4^\circ\text{C}$ , and  $A_y = 16^\circ\text{C}$ .

Table 3: Depths for a daily temperature wave ( $X_d$ ) and an annual wave ( $X_y$ ) where the amplitude has been reduced to  $A_z$ .

$A_z (^\circ\text{C})$	0.200	0.100	0.050	0.020	0.010	0.001
$X_d \text{ (m)}$	0.34	0.44	0.54	0.68	0.78	1.12
$X_y \text{ (m)}$	12.36	14.32	16.27	18.86	20.81	27.31

Experience with models I and II suggests that, in general,  $\Delta x$  and  $\Delta t$  should be made small with  $\Delta x \ll X$ , the depth of interest,  $\Delta t \ll P$  (period or duration of surface temperature change),  $\Delta_{xx}T \gg \delta(\Delta_{xx}T)$  and  $\Delta'_{xx}T \gg \delta(\Delta'_{xx}T)$ . For the active layer, these considerations and Table 3 suggest that  $\Delta x$  can range from a few centimeters to a tenth of a meter or so and  $\Delta t$  can range from a few minutes to an hour or so. At deeper depths but within the depth of annual temperature variations,  $\Delta x$  can range from a few tenths of a meter to about one meter and  $\Delta t$  from one day to several weeks.

## SUMMARY

The purpose of this paper is to investigate numerical methods for determining the *in situ* thermal diffusivity,  $D$ , of the active layer and permafrost from a temperature time series. When the active layer and permafrost contain unfrozen water, the thermal parameters become strongly dependent upon temperature. In this case, it is shown that

$$D = \frac{T_t}{T_{xx} - RT_z^2(-T)^{B-1}} \quad (8)$$

where  $T$  is the temperature,  $T_t$ ,  $T_z$  and  $T_{xx}$  are the numerical approximations of

$\partial T/\partial t$ ,  $\partial T/\partial x$ , and  $\partial^2 T/\partial x^2$ , respectively, B is a constant and R is defined in the text. Application of (8) requires a knowledge of the variation of unfrozen water,  $\theta_u$ , and R with temperature.

Previous investigators have used the first order numerical expression for D for the case of constant thermal parameters, termed model I, which is

$$D \cong \left( \frac{(\Delta x)^2}{2\Delta t} \right) \frac{\Delta_t T}{\Delta_{xx} T} \quad (12)$$

where  $\Delta x$  is the space step,  $\Delta t$  is the time step,  $\Delta_t T = T_i^{j+1} - T_i^{j-1}$ ,  $\Delta_{xx} T = T_{i-1}^j - 2T_i^j + T_{i+1}^j$ , and the integers  $i$  and  $j$  reference positions and time. A second order approximation of the derivatives  $T_t$  and  $T_{xx}$  was developed using a Taylor series expansion, termed model II, which yields

$$D \cong \left( \frac{(\Delta x)^2}{\Delta t} \right) \frac{\Delta'_t T}{\Delta'_{xx} T} \quad (16)$$

where  $\Delta'_t T = T_i^{j-2} - 8T_i^{j-1} + 8T_i^{j+1} - T_i^{j+2}$  and  $\Delta'_{xx} T = -T_{i-2}^j + 16T_{i-1}^j - 30T_i^j + 16T_{i+1}^j - T_{i+2}^j$ .

In addition to the obvious requirement for conductive heat flow, they are several considerations in applying (12) and (16) to determine D. The spatial separation,  $\Delta x$ , of the temperature measurements (sensors) and the time intervals,  $\Delta t$ , between measurements must be relatively small and the soil in either a frozen or thawed state. Estimates of  $\Delta_t T$  and  $\Delta'_t T$  are nearly independent of sensor accuracy while  $\Delta_{xx} T$  and  $\Delta'_{xx} T$  depend on sensor accuracy. Temperature changes at depth should be sufficient to make  $\Delta_{xx} T$  and  $\Delta'_{xx} T$  much greater than the errors in their determination.

The higher order approximations used for  $T_t$  and  $T_{xx}$  in model II result in smaller truncation errors which makes model II much more accurate than model I. However, there are also measurement errors associated with the temperatures, positions, and time. An error analysis shows that the measurement errors are dominated by errors in the temperature measurements. For a given level of accuracy in the temperature measurements, the measurement errors for model I are somewhat less than those for model II. The analysis also shows that the accuracy of the temperature measurements must approach  $\pm 0.01^\circ\text{C}$  to obtain reasonable estimates of D.

Additional information on the application of model I and model II was obtained by using surface temperatures consisting of a daily wave, an annual wave with a super-

imposed daily wave, and an annual wave with a superimposed linear trend to generate synthetic temperature time series in the ground. Calculated values of  $D$  using (12) and (16) were then compared to the input value used to calculate the synthetic temperature profiles. The percent difference between the calculated values and the input value is the error in the calculations.

For a daily wave, model I produces large spikes in the calculated values for  $D$ . These spikes occur near times where  $T$  is a maximum or a minimum and  $\Delta_t T$  and  $\Delta_{xx} T$  become very small. Using model II, the spikes disappear and the errors are also much smaller at other times. These improved estimates using model II are due to the reduction in truncation errors compared to model I. Round off errors do not appear to be significant for either model for the parameters used in the calculations.

For a daily wave superimposed on an annual wave, the effect of the annual wave is not significant at shallow depths (up to 0.5 m in the example calculation). At these depths, the results for  $D$  were similar to those for a daily wave only. As the amplitude of the daily wave increased, the errors in  $D$  increased and as the depth increased to 1.2 m and beyond the errors decreased. At a depth of 0.8 m, calculated values for  $D$  using model I resulted in a series of spikes near the temperature maximum and minimum and normal values elsewhere. These spikes were produced by the daily temperature variations which caused the temperature dependent quantities on the right sides of (12) and (16) to oscillate about zero for a period of time. The number of spikes, their amplitude, and duration were substantially reduced using model II. At a depth of several meters to 20 m or more, model I produced values for  $D$  which were in error by less than 20%. However, when model II was used, the values for  $D$  were nearly identical to the input value.

An annual surface wave with a superimposed linear trend, which could be caused by climatic fluctuations, was used to show that  $D$  could be obtained at depths below those of annual variations (about 35 m for this example). The errors in values for both models I and II were less than 2% with model II being more precise.

Values for  $D$  can be obtained at any depth where measurable temperature changes occur. Short term weather patterns, the presence of a freezing or thawing front in the active layer, and longer term climatic fluctuations and trends create opportunities for determining  $D$ . Application of the method requires the acquisition of very precise temperature data (preferably  $\pm 0.01^\circ\text{C}$  or better) at appropriate depth ( $\Delta x$ ) and time ( $\Delta t$ ) intervals. Selection of values for  $\Delta x$  and  $\Delta t$  must take into account the accuracy

of the temperature measurements, duration and amplitude of the temperature changes, depth where  $D$  is to be determined, and the diffusivity of the soil. In general,  $\Delta x \ll X$  (the depth of interest),  $\Delta t \ll P$  (period or duration of surface temperature changes), and  $\Delta_{xx}T$  and  $\Delta'_{xx}T$  much greater than the errors in their determination. For the active layer,  $\Delta x$  can range from a few centimeters to a tenth of a meter or so and  $\Delta t$  from a few minutes to an hour or so. At deeper depths in the permafrost but within the depth of annual temperature variations,  $\Delta x$  can range from a few tenths of a meter to a meter or more and  $\Delta t$  from one day to several weeks. Below the depth of annual temperature variations, values for  $\Delta x$  of several meters and  $\Delta t$  of a year or more may be appropriate. The method is not limited to permafrost regions and should be applicable to any soil or rock where the heat flow is conductive.

### Acknowledgements

We wish to thank Dr. Z. Kowalik for his helpful discussions. This research was funded by the National Science Foundation grant DPP 91-22928, Army Research Office grant DAAL03-89-K-0106, State of Alaska funds and by the Lanzhou Institute of Glaciology and Geocryology, Chinese Academy of Sciences, People's Republic of China.

## REFERENCES

- Carnahan, B., H. A. Luther and J. O. Wilkes *Applied Numerical Methods*, 604 pp., John Wiley & Sons, Inc., New York, 1969.
- Carslaw, H. S. and J. E. Jaeger, *Conduction of Heat in Solids*, 510 pp., 2nd edition, Oxford University Press, New York, 1959.
- Gerald, C. F. and P. O. Wheatley, *Applied Numerical Analysis*, 679 pp., 4th Edition, Addison-Wesley Publishing Company, New York, 1989.
- Guymon, G.L., T. V. Hromadka II, and R. L. Berg, Two dimensional model of coupled heat and moisture transport in frost-heaving soil materials. *J. Energy Resour. Technol.*, 106, 336-343, 1984.
- Hinkel, K. M., S. I. Outcalt, and F. E. Nelson, Temperature variation and apparent thermal diffusivity in the refreezing active layer, Toolik Lake, Alaska. *Permafrost and Periglacial Processes*, 1, 265- 274, 1990.
- McGaw, R. W., S. I. Outcalt, and E. Ng, Thermal properties of wet tundra soils at Barrow, Alaska. In *Proceedings Third International Conference on Permafrost, Edmonton, Alberta*. National Research Council of Canada, Ottawa, Vol. 1, 47-53, 1978.
- Nelson, F. E., S. I. Outcalt, C. W. Goodwin, and K. M. Hinkel, Diurnal thermal regime in a peat-covered palsa, Toolik Lake, Alaska. *Arctic*, 38(4), 310-315, 1985.
- Osterkamp, T. E., Freezing and thawing of soils and permafrost containing unfrozen water or brine, *Water Resources Research*, 23(12), 2279-2285, 1987.
- Outcalt, S. I., and K. M. Hinkel, Night frost modulation of the near-surface soil water ion concentration and thermal fields. *Physical Geography*, 10(4), 336-348, 1989.
- Outcalt, S. I., and K. M. Hinkel, The soil electric potential signature of summer drought. *Theoretical and Applied Climatology*, 41(1), 63-68, 1990.
- Zhang, T., *Thermal Regime of Permafrost Within the Depth of Annual Temperature Variation at Prudhoe Bay, Alaska*, pp. 145, MS thesis, Geophysical Institute, University of Alaska Fairbanks, 1989.

## Figure Captions

Figure 1. (A) Synthetic temperature time series at three depths for a daily surface temperature wave with a surface amplitude of  $4^{\circ}\text{C}$ , (B)  $\Delta_{xx}T$  and  $\Delta_t T$  at the central depth of 0.3 m, and (C) a comparison of the calculated values of the thermal diffusivity at the 0.3 m depth with the input value of  $25 \text{ m}^2 \text{ yr}^{-1}$ . For these calculations,  $\Delta x = 0.1 \text{ m}$ ,  $\Delta t = 10 \text{ min}$ .

Figure 2. Variations of the calculated thermal diffusivity at a depth of 0.3 m for different values of  $\Delta x$  and  $\Delta t$ : (A)  $\Delta x = 0.01 \text{ m}$  and  $\Delta t = 60 \text{ min}$ , (B)  $\Delta x = 0.10 \text{ m}$  and  $\Delta t = 1 \text{ min}$ , and (C)  $\Delta x = 0.01 \text{ m}$  and  $\Delta t = 1 \text{ min}$ .

Figure 3. (A) Five synthetic temperature profiles for depths below the daily zero temperature variation and, (B), a comparison of the calculated values between models I and II. For these calculations,  $A_d = 4^{\circ}\text{C}$ ,  $\Delta x = 1 \text{ m}$ , and  $\Delta t = 5 \text{ days}$ .

Figure 4. (A) Five synthetic temperature profiles, calculated after ten years, for a warming trend of ground surface temperature with a superimposed annual surface temperature wave and, (B), a comparison of the calculated thermal diffusivities from the temperature profiles. For the temperature calculations,  $A_y = 16^{\circ}\text{C}$ ,  $\Delta x = 1 \text{ m}$ , and  $\Delta t = 1 \text{ year}$ , and for the thermal diffusivity calculations,  $\Delta x = 4 \text{ m}$  and  $\Delta t = 1 \text{ year}$ .

